Nano-structured bismuth tungstate with controlled morphology: fabrication, modification, environmental application and mechanism insight

Huan Yi [a,b,1], Lei Qin [a,b,1], Danlian Huang [a,b,1], Guangming Zeng [a,b,*], Cui Lai [a,b,*], Xigui Liu [a,b], Bisheng Li [a,b], Han Wang [a,b], Chengyun Zhou [a,b], Fanglong Huang [a,b], Shiyu Liu [a,b], Xueying Guo [a,b]

[a]*College of Environmental Science and Engineering, Hunan University, Changsha, Hunan 410082, China*

[b]*Key Laboratory of Environmental Biology and Pollution Control (Hunan University), Ministry of Education, Changsha, Hunan 410082, China*

*Corresponding author at: College of Environmental Science and Engineering, Hunan University, Changsha, Hunan 410082, China (G.M. Zeng and C. Lai).

Tel.: +86–731– 88822754; fax: +86–731–88823701.

E-mail address: zgming@hnu.edu.cn (G.M. Zeng), laicui@hnu.edu.cn (C. Lai).

1 These authors contribute equally to this article.

Contents

1. Introduction

2. Controllable fabrication of nano-structured BWO

2.1 Three-dimensional structured BWO

2.2 Two-dimensional structured BWO

2.3 One-dimensional structured BWO

3. Modification of nano-structured BWO

4. Environmental application of nano-structured BWO

4.1 Application in environmental pollutant treatment

4.1.1 Oxidation of organic pollutants

4.1.2 Treatment of inorganics

4.2 Application in clean-energy production

4.2.1 Fuel energy production

4.2.2 Hydrogen production

5. Summary and prospects

5.1 Summary

5.2 Challenges and prospects

Abstract

Bismuth tungstate with different structures and morphologies show different properties. The structure and morphology have been proven to be critical factors to tune the electronic properties to influence photocatalytic performance. Notably, nano-structured bismuth tungstate were found to exhibit high activity in photocatalytic degradation process. Controllable fabrication on nano structures with desired morphology is indispensable to achieve the related properties well. However, a review that declare the correlation between the property and the fabrication, structure and morphology of bismuth tungstate is still absent. Therefore, we firstly summarize a series of recent fabrication methods for various dimensional nano structures of bismuth tungstate. Then the modification of nano-structured BWO to improve the photocatalytic performance are presented, including morphological manipulation, doping or substitution, solid solution fabrication, and compound formation. The mechanism of photocatalytic oxidation and reduction process over nano-structured bismuth tungstate is also explored, especially the role of radical species. Additionally, advanced environmental application are summarized. Finally, unresolved challenges and potential applications of nano-structured bismuth tungstate are presented for future research directions.

Key words: Bismuth tungstate; Nano structure; Photocatalysis; Environmental pollutant treatment; Clean-energy production.

1. Introduction

Due to the more serious energy and environmental issues, efficient methods for environmental application are in a great demand [1-8]. Many common technologies such as biotreatment [9-11], electrochemical process [12], oxidation process [13, 14], magnetic separation [15], adsorption [16-18], and designed nanotechnology [19-21] have been used to address these problems but without desired efficiency. In recent years, photocatalysis has been developed as a highly-efficient solution [22-25]. Some photocatalytic materials in the past few decades revealed high photocatalytic activity but only under UV irradiation due to the wide band gap, like titanium dioxide (TiO_2) [26-29]. Afterwards, from the viewpoint of full use in solar energy, considerable attention has been paid to the exploration of a wider range of light active photocatalysts [30]. Binary metal oxides composed of metal cations, such as ZnO, Fe_2O_3 and Ag_2O, are prior visible light-active photocatalysts, but limited by photocorrosion [31-33]. Subsequently, emerging ternary metal oxides as visible light-active photocatalysts have been developed [34-36].

Bismuth tungstate (BWO), a ternary metal oxide, has been one of the most studied visible light-driven photocatalysts in recent years owing to its benefits of wide spectrum light response and no secondary contamination after utilization [37, 38]. BWO shows visible-light absorption edge around 470 nm with band gap located at ~2.8 eV. BWO is constructed of perovskite-like $[WO_4]^{2-}$ layers sandwiched between $[Bi_2O_2]^{2+}$ layers. Such structure is beneficial for separating photoexcited electron-hole pairs and forming internal electric fields between the slabs, and then enhancing the photocatalytic performance (Fig. 1) [39, 40]. Valence band (VB) of BWO is formed by O 2p and Bi 6p with a minor assistance from Bi 6s hybrid orbitals, while conduction band (CB) of BWO is composed by W 5d with the assistance from Bi 6p orbitals. The hybridization of Bi 6s and O 2p leads to a largely dispersed VB, accelerating the mobility of photoexcited holes and enhance the oxidation capability.

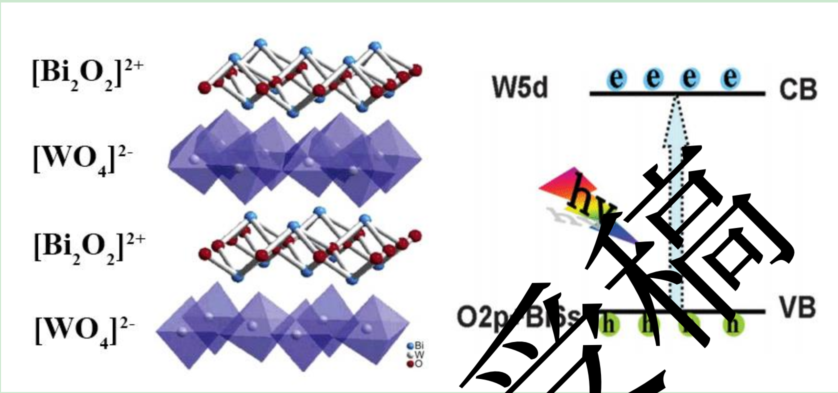

Fig. 1 Composition and band structure of BWO. Reprinted from ref [39] with permission from The Royal Society of Chemistry.

BWO was first prepared through conventional solid state reaction and used for oxygen evolution [41]. Up to date, BWO has been synthesized via various ways, such as sol-gel process, ultrasound induced aggregation, calcination, precipitation, microemulsion, and hydro-/solvo-thermal process [42-52]. The properties of BWO with diverse structures and morphologies are substantially different [53]. As a result, development of controlled structures and morphologies to enhance photocatalytic performance of BWO has be one of the recent hotspots. Particularly, nano-structured BWO assemblies are believed to show excellent catalytic performance because of the large surface area and efficient separation of charge carriers. Previously, Zhang et.al [54] reviewed the visible-light-driven photocatalytic applications of BWO. Soon after that, Zhu et.al [55] summarized the controllable synthesis and enhancement of visible-light-driven photocatalytic performance of BWO nanoplates and highly porous films. Then in the year 2014, Pagliaro et.al [39] described the progress in selective organic synthesis and fuel production over BWO. However, for further development, an updated comprehensive overview on controllable fabrication, modification, and advanced environmental application of BWO focusing on tuning nano structure and morphology is urgently needed.

This review aims at declaring the correlation between the property and the fabrication, structure and morphology of bismuth tungstate. Therefore, we firstly review the updated fabrication methods for nano structures of BWO, along with discussing the significant factors that determining the formation of morphology (e.g. the precursor, temperature, reaction pH and time, solvent or surfactant). Differences in the photocatalytic performance of different dimensional nano-structured bismuth tungstate are emphatically discussed. Then the modification of nano-structured BWO to improve the photocatalytic performance are presented, including morphological manipulation, doping or substitution, solid solution fabrication, and heterojunction construction. Advanced environmental application and the comparison in photocatalytic activity of pure nano-structured BWO and modified BWO composites are also summarized. Additionally, we explore the mechanism that photocatalytic activity varies with changed morphology of BWO, especially the role of active species, such as hydroxyl radicals, superoxide radical, and photoexcited holes. Finally, we discuss the challenges of nano-structured BWO applied in photocatalysis or even wider fields, and future research directions.

2. Controllable fabrication of nano-structured BWO

BWO with the same composition but different morphologies could be substantially different. Both size and morphology have an effect on the photocatalytic performance of BWO. For example, nano-scale BWO photocatalysts generally perform better than the bulk owing to the more active sites and separation efficiency of charge carriers; and hierarchical BWO photocatalysts show several superiorities: (i) micrometer scale that benefit easy separation and recycle, (ii) special wettability in some cases that is good for special reaction system, (iii) high photocatalytic activity as nanounits, (iv) quick transportation of reactants to the surface owing to the abundant interspaces formed among adjacent nanounits, and (v) efficient light adsorption because of light multireflection. Moreover, the morphology of nano-structured BWO have a significant influence in the physical properties. When the radial dimension of nano-structured BWO belongs to a characteristic size, phonon mean-free path and quantum mechanical effects will change, which have a significant influence in the photocatalytic performance.

2.1 Three-dimensional structured BWO

Three-dimensional (3D) nano-structured BWO assemblies have received wide attention owing to the fascinating architecture and characteristics. And because the superstructure benefits the photocatalytic process and recycling process of BWO, the fabrication of 3D nano-scale hierarchical structure is popular. There are various 3D nano structures of BWO, such as flower-like or flake ball-shaped structure, hierarchical microsphere, nano-structured particles with porous nanoplates, and porous hollow structure. Copious synthesis methods for 3D nano-structured BWO have been developed, like hydro-/solvo-thermal process, mechanical exfoliation, sol-gel process, chemical vapour deposition (CVD), solid-state reaction, and microwave-assisted method [46, 56, 57]. Overall, the precursor, reaction temperature, pH, solvent or surfactant have an impact on the formation of BWO.

(i) Flower-like or flake ball-shaped BWO superstructures. BWO with 3D flower-like structure can be fabricated via facile hydrothermal process [58]. In our method, $Bi(NO_3)_3 \cdot 5H_2O$ and $Na_2WO_4 \cdot 2H_2O$ were used as precursors. Generally, $Bi(NO_3)_3 \cdot 5H_2O$ was dissolved in 1.0 M HNO_3, and $Na_2WO_4 \cdot 2H_2O$ was dissolved in 1.0 M NaOH. Afterwards, the Na_2WO_4 solution was added dropwise into the $Bi(NO_3)_3$ solution, and adjust the solution pH to 4. Finally, the suspension was heated at 140 ℃ for 20 h. The obtained 3D flower-like BWO showed high photocatalytic degradation on rhodamine b (RhB) [58]. A three-step formation mechanism for the flower-like BWO superstructures has been presented by Zhang et.al [59]: self aggregation, dissolution-recrystallization process, and self organization (Fig. 2).

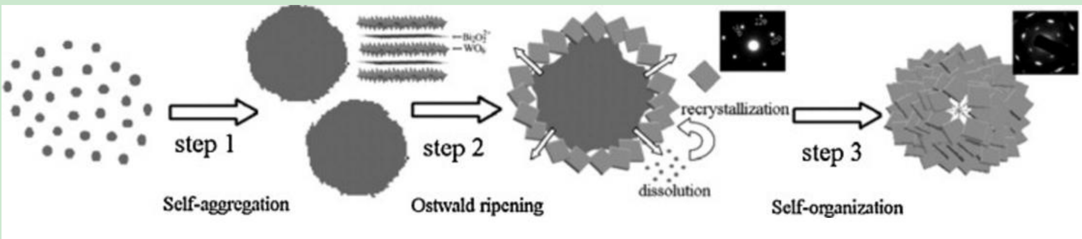

Fig. 2 Three-step formation mechanism for the flower-like BWO superstructures. Reprinted from ref [59] with permission from The Royal Society of Chemistry.

(ii) Hierarchical BWO microspheres. A 3D hierarchical BWO microsphere assembled by nanoplate alignment was prepared via a mixed sol-gel hydrothermal process [60]: firstly mix $Bi(NO_3)_3$ and Na_2WO_4 EDTA solution, then evaporate at 80 ℃, finally keep heating at 200 ℃ for 24 h. Hierarchical BWO microspheres can improve the efficiency of light absorption because of the increase in the number of active sites caused by the higher surface areas. According to the photocatalytic degradation experiment, about 80% of 10 mg L^{-1} MB can be degraded in 100 min over 0.67 g L^{-1} of 3D hierarchical BWO microspheres [60].

(iii) Nano-structured BWO nanoparticles. A 3D BWO nanoparticles was prepared successfully via a microwave-assisted method [61]. The whole microwave-assisted process includes three steps: firstly mix $Bi(NO_3)_3$ and Na_2WO_4 water solution, then heat by a microwave oven for 20 min, lastly keep annealing at 500 ℃ for 5 h in air. The obtained 3D BWO nanoparticles (~60 nm) show a large surface area (14.6 m^2 g^{-1}) and a high transportation efficiency of photogenerated charge carriers. Additionally, the photocatalytic degradation efficiency of 10^{-5} M MB achieved 92% in 180 min over 1 g L^{-1} of BWO photocatalysts [61].

(iv) Porous hollow structures. A porous hollow BWO nanocage constructed by minor nanoparticles (50-80 nm) was prepared via a simple refluxing process in ethylene glycol (EG) [62]. EG was employed to generate the complex of Bi^{3+} or WO_4^{2-} with hydroxyl groups via coordination reaction. And then the complex decomposed to release the meal ions to form BWO grains in the refluxing EG solution with using carbon spheres as the template. Finally, nanocage BWO built by these BWO grains was formed after a calcination process. The obtained nanocage BWO exhibit great visible-light-driven catalytic activity, and the photodegradation of RhB over nanocage BWO achieved nearly 100% in 50 min. Additionally, it is easy for them to get separation and recycling owing to the rapid natural subsidence.

2.2 Two-dimensional structured BWO

Compared with 3D nano-structured BWO, two-dimensional (2D) nano-structured BWO are believed to perform better in photocatalytic process [63, 64]. This is because the photogenerated electron-hole pairs in 2D structure can come up to the surface more quickly than that excited deeply in 3D structure, which is conducive to the separation of electron-hole pairs and enhancement of the photocatalytic performance [65-67]. And once the thickness of BWO decreases to single unit cell, there is an increased density of states at CB edge. Moreover, ultrathin BWO layers revealed higher efficiency in light absorption owing to the remarkable large surface area that allowed quick absorption [38, 68]. Recently, the various monolayers can be stacked via van der Waals forces and/or chemical bonds. Notably, chemical bonding can significantly improve charge separation efficiency, and even induce the production of new energy band. A monolayer structure is considered as the stack of monolayer BWO constructed via chemical bonds, and possesses oxygen-depleted surface with abundant active sites [69].

(i) nano-structured BWO nanoplates. The square BWO nanoplates were firstly prepared via a hydrothermal process, which was presented by Zhu et.al [70].The neutral aqueous solution consisting of $Bi(NO_3)_3$ and Na_2WO_4 was heated at 120-240 ℃ for 20 h. Tiny crystalline nuclei was firstly formed in a supersaturated medium. Then the crystal grew at the expense of small irregular nanoparticles owing to the energy difference in solubility. As the reaction continued, irregular nanoparticles began to dissolve, and large BWO nanoplates were formed via anisotropic growth of laminar structure along (001) plane parallel to the intrinsic layered structure. The obtained BWO nanoplates showed excellent photocatalytic activity. This is because the large surface area of BWO nanoplates expand the reaction sites, and the laminar structure benefits the photogenerated electron-hole separation.

(ii) BWO microdiscs. The 2D BWO microdiscs consisting of square nanoplates, which were stacked together in a side-by-side way. They were prepared through a hydrothermal process with the assistance of acetic acid. Mix $Bi(NO_3)_3$ acetic acid solution and Na_2WO_4 water solution and then keep heating at 180 ℃ for 12 h. The obtained BWO revealed a high surface area (26.1 m^2g^{-1}), and show a high photocatalytic degradation efficiency of RhB owing to the structure built by layer-by-layer grew nanoplates [71].

(iii) Porous BWO nanoplates. A sol-gel process with egg white proteins (albumin) as biotemplate was used for the fabrication of porous BWO nanoplates with thickness of ~100 nm [72]. In the sol-gel process, the gelata is a key factor in the mineralization that determines the structure and diameter size of BWO photocatalysts. Porous structure reveals higher active surface area and better adsorptivity, and nanoplate-like structure allowed multiple reflections of irradiation light that improved light absorption efficiency [72].

(iv) Ultrathin monolayer BWO. Commonly, monolayer BWO can be produced via an alternative bottom-up approach or liquid exfoliation of the van der Waals layered materials. In the fabrication of monolayer structure, the key is to stay monolayers from stacking together. Recently, a cetyltrimethylammonium bromide (CTAB)-assisted bottom-up process was developed to prepare ultrathin 2D monolayer BWO (m-BWO) nanosheets with $[BiO]^{+}$-$[WO_4]^{2-}$-$[BiO]^{+}$ sandwich substructure (Fig. 3) [73]. Br ions from CTAB were adsorbed on the surface, and then made the monolayers negatively charge and induced a decrease in the band gap energy of m-BWO nanosheets. The hydrophobic chains of CTA^{+} ions blocked the stacking of monolayers with the assistance of Coulomb repulsion forces. Bi atoms on the surface of monolayers were coordinatively unsaturated, which increased the active sites.

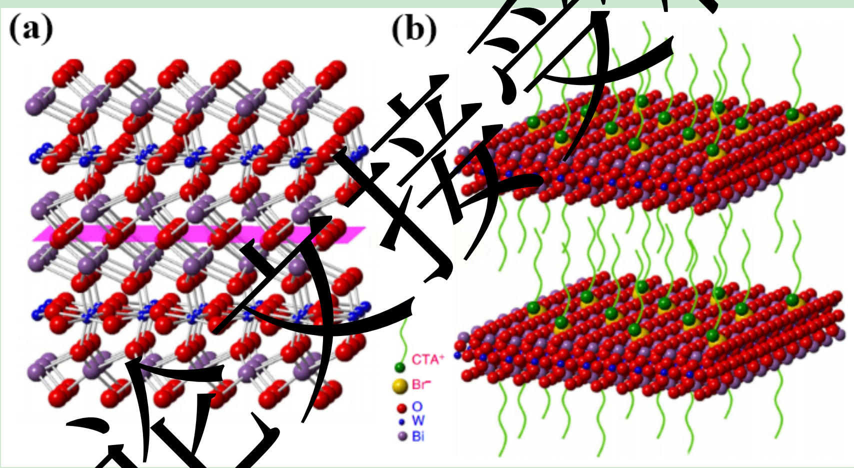

Fig. 3 (a) Crystal structure of BWO; (b) proposed mechanism of the m-BWO with the assistance of Br^{-} ions. Reprinted from ref [73] with permission from Nature.

2.3 One-dimensional structured BWO

Various dimensional nano-structured BWO photocatalysts have been synthesized. Among them, one-dimensional (1D) nano structures of BWO are promising to play key roles on the horizon of material science, and be applied in photocatalysis because of the fascinating geometric characteristics, optical and electronic properties [74, 75].

Different from 3D and 2D BWO, 1D nano-structured BWO exhibit obvious chemical and structural behaviour owing to the high length-to-diameter ratio and exclusive two-dimensional confinement. The high length-to-diameter ratio benefits the transfer of quantum particles (including photons, phonons and electrons) so that 1D nano structures can control many different forms of energy transport. 1D nano structures of BWO photocatalysts have been fabricated successfully.

(i) Thread-like BWO. 1D thread-like BWO was prepared via a hydrothermal process with $NH_3{\cdot}H_2O$ as alkaline source and reaction pH located at 1 [76]. The $Bi(NO_3)_3 \cdot 5H_2O$ and $Na_2WO_4 \cdot 2H_2O$ precursor HNO_3 solution went through a 24 h of thermal treatment at 180 ℃. The obtained thread-like BWO shows high BET surface area (12.16 m^2 g^{-1}). And the photocatalytic degradation of RhB over the thread-like BWO achieved 78.2% in 50 min [76].

(ii) Hierarchical BWO hollow tubes. 1D hierarchical BWO hollow tubes have been prepared via a solvothermal process with using Bi_2O_3 rods as both templates and reactant treated at 120 ℃ for 6 h (Fig. 4) [77]. And an interesting macro-mesoporous structure was formed by BWO nanoplates stacking in a disordered state. The porous structure increases the surface areas to show more reaction sites, and supplies more pathways for molecule diffusion. Additionally, the design of 1D hollow structure can significantly improve the charge collection because the photogenerated electrons and holes travel faster along the unique 1D channel [78]. According to the experimental result, the 1D BWO hollow tubes show high activity on RhB photodegradation of with the degradation efficiency obtained 99.0% in 90 min [77].

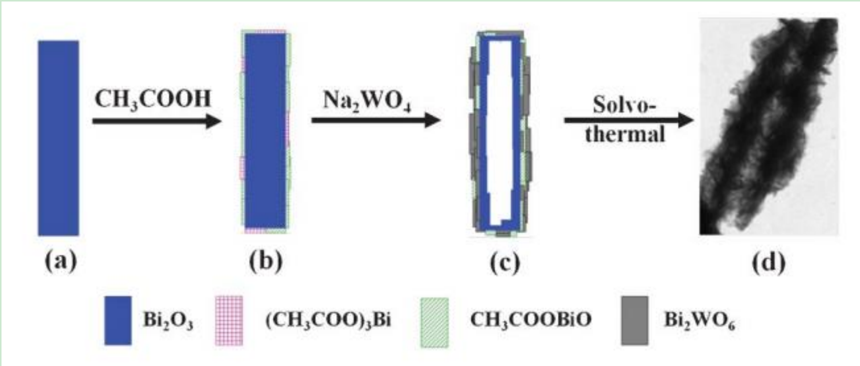

Fig. 4 Formation mechanism of 1D hierarchical BWO hollow tubes. Reprinted from ref [77] with permission from The Royal Society of Chemistry.

Different dimensional nano-structured BWO can be fabricated via various methods, which have been summarized in Table 1. In controllable fabrication process of nano-structured BWO, there are many influencing factors, including pH value of precursor solution, reaction temperature and time, nature of surfactant, metal precursor, and alkaline source. Structure and morphology control provides a versatility for adjusting the optical and electric properties of BWO. For higher photocatalytic efficiency of BWO in application, the first is to develop applicative methods for the controllable fabrication of different dimensional nano-structured BWO to tune the photocatalytic properties.

3. Modification of nano-structured BWO

The photocatalytic performance of nano-structured BWO depends on its intrinsic properties. Major limitations for pure nano-structured BWO applied in photocatalytic process are the high recombination of photogenerated electron-hole pairs and limited photoabsorption range [79]. To enhance the catalytic activity of nano-structured BWO for environmental pollutant treatment and clean-energy production, there are mainly four efficient methods.

(i) Morphological manipulation. Increase the exposure of highly reactive surfaces on crystals by modifying the physical morphology is an alternative strategy to improve the photocatalytic performance of nano-structured BWO [80]. The increased exposure of high-energy facets can improve the photoelectric and optical properties of BWO, which can also suppress the recombination of charge carriers. Besides, the interaction between the reactive surfaces and reactant substances and various types of surface defects have an impact on the photocatalytic performance. A BWO nanobipyramids with high density of high-energy facets was prepared via a facile solvothermal process, showing enhanced solar-driven photoactivity compared with flower-like BWO structures (Fig. 5) [80]. The surface defects played as the absorption sites for charge carriers to be transferred to the adsorbed substances, which improve the separation of charge carriers and photocatalytic performance.

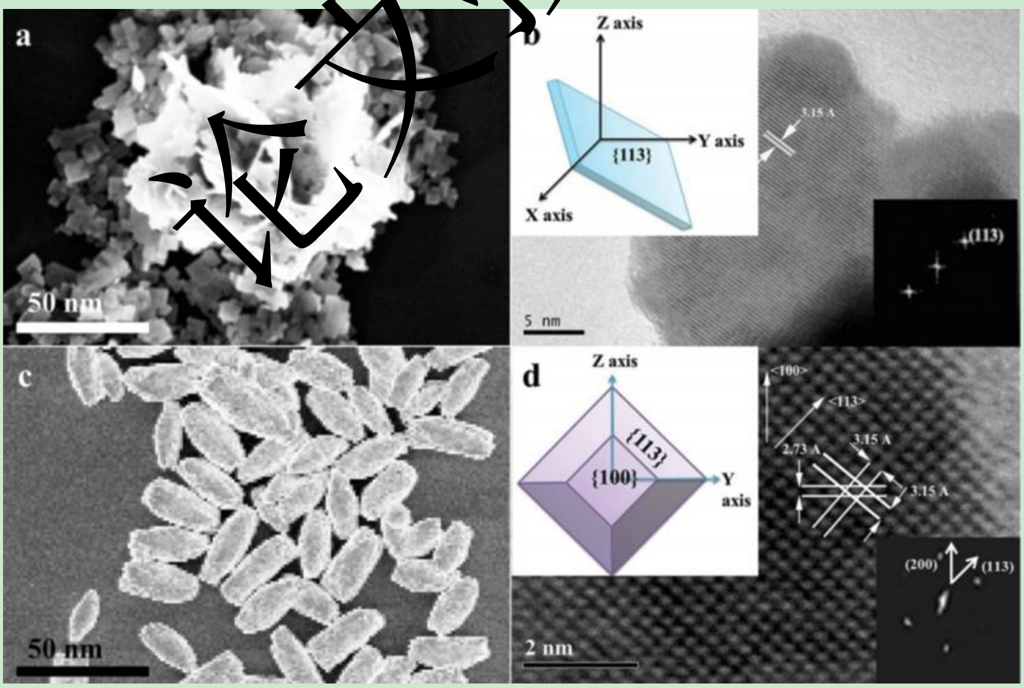

Fig. 5 (a) SEM and (b) HRTEM images of flower-like BWO structures (hydrothermal synthesis, pH=1); (c) SEM and (d) HRTEM images of BWO nanobipyramids.

Reprinted from ref [80] with permission from Wiley.

(ii) Doping or substitution. Doping nano-structured BWO with other elements can affect the optical properties via narrowing the electronic properties. The electronic properties have a significant influence in the atomic arrangement and physical dimension for BWO nano structures. So far, much effort has been devoted to BWO doping or substitution with metal (e.g. Fe, Mn, Ag and Mo) and nonmetal (e.g. F, Cl, Br and N) elements. Very recently, an iron-doped BWO was presented to show excellent photocatalytic performance [81]. Appropriate amount of oxygen vacancies in iron-doped BWO benefits the improvement of photocatalytic performance (Fig. 6) [81]. The oxygen vacancies can make dopant energy levels close to the CB edge of BWO, which extend the region of irradiation light photo-response and decrease the recombination of photogenerated electron-hole pairs. Additionally, the oxygen vacancies can play as electron-rich centers to enhance the absorption of photodegradation substrates.

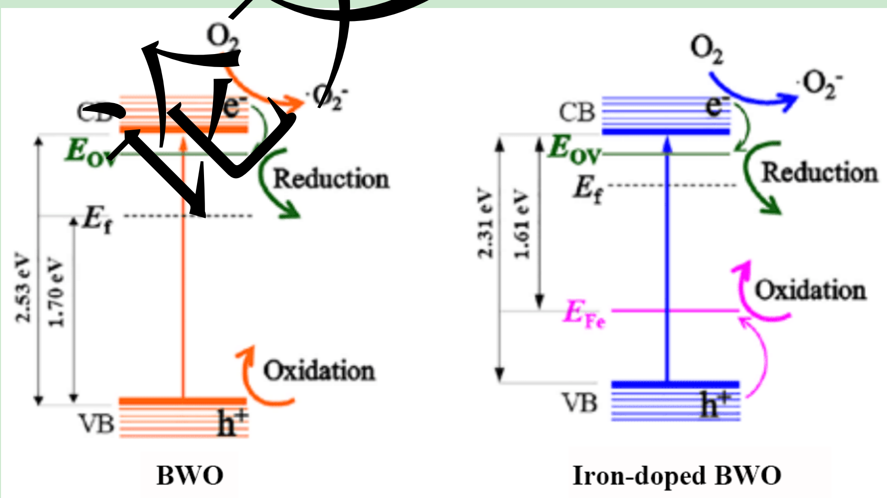

Fig. 6 Energy band structures and charge transfer process of BWO and iron-doped BWO (E_f, Fermi level; E_{OV}, the energy level of oxygen vacancies; E_{Fe}, the iron doping energy level). Reprinted from ref [81] with permission from Wiley.

(iii) Solid solution fabrication. The solid solution fabrication not only can improve the visible-light absorption and electron transportation efficiency, but also can precisely tailor the band gap and optoelectronic properties of BWO to achieve an optimal balance between the photoabsorption and redox potentials [82] . The ions in host material can be replaced and the concentration can be controlled for a tunable property [83]. Therefore, the doped element is crucial for desired properties. Solid solution fabrication of BWO show many superiorities, like large surface area, high quantum confinement effect and size effect [84, 85]. In the formation of BWO solid solution nanostructure, three factors merit attention for low formation energy and broad composition tuning: crystallographic parameters, chemical valance, and radius cations or anions [86]. After tremendous efforts, BWO solid solution nanostructures with various desired morphologies have been fabricated successfully, which achieved great progress in precise regulation of band gap and photoelectrical properties. For example, a $Bi_2Mo_xW_{1-x}O_6$ solid solution with tunable band structure was prepared, and showed improved catalytic activity (Fig. 7) [85]. WO_4^{2-} and MoO_4^{2-} ions firstly absorbed on the surface of BiOBr, and then replaced the Br^- ions. As the reaction continued, a hollow structure was formed.

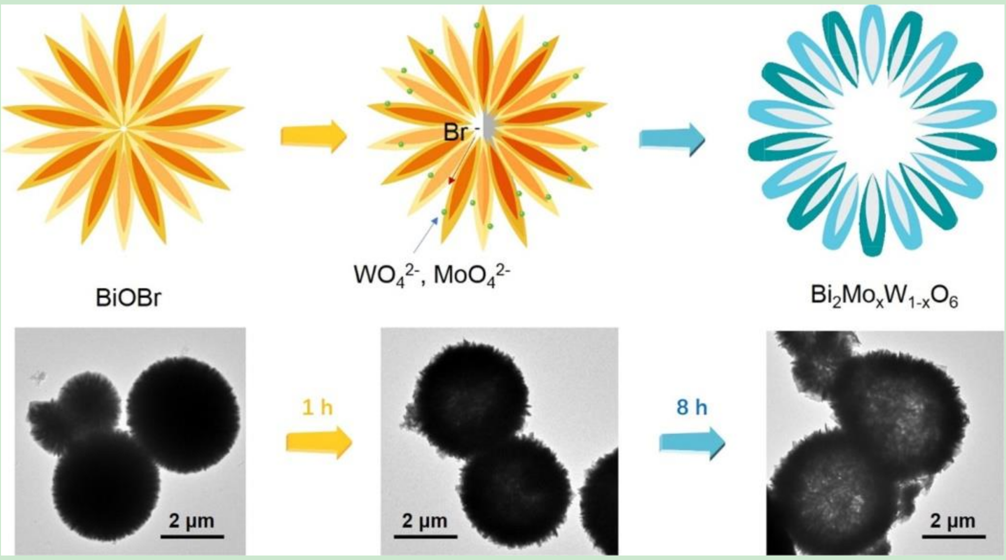

Fig. 7 Formation process of $Bi_2Mo_xW_{1-x}O_6$ solid solutions from BiOBr. Reprinted from ref [85] with permission from Elsevier.

(iv) Compound formation. The formation of compound, like heterojunction, with expected band potentials and wide photoabsorption range is an efficient method to enhance the catalytic performance of nano-structured BWO in environmental and energy fields [50, 87, 88]. Nano-structured BWO can integrate with other substances to form heterojunctions, and novel nanostructures can be obtained to separate the photogenerated charge carriers [89-91]. Appropriate band positions of two components are required for the energy level offsets in heterojunction construction, so that the space charge at the interfaces can accumulate and then enhance the charge separation [92]. Recently, we prepared a visible-light-driven $Bi_2Fe_4O_9/Bi_2WO_6$ (BFWO) composite via one-step hydrothermal method [93]. The obtained BFWO heterojunctions have an extraordinary enhancement in photocatalytic performance compared with pure BWO. In the photocatalytic process, the photogenerated charge carriers transfer process was fit the Z-scheme charge transfer system (Fig. 8) [93]. Therefore, the photoexcited charge carriers can be efficiently separated and then the photocatalytic activity was significantly enhanced.

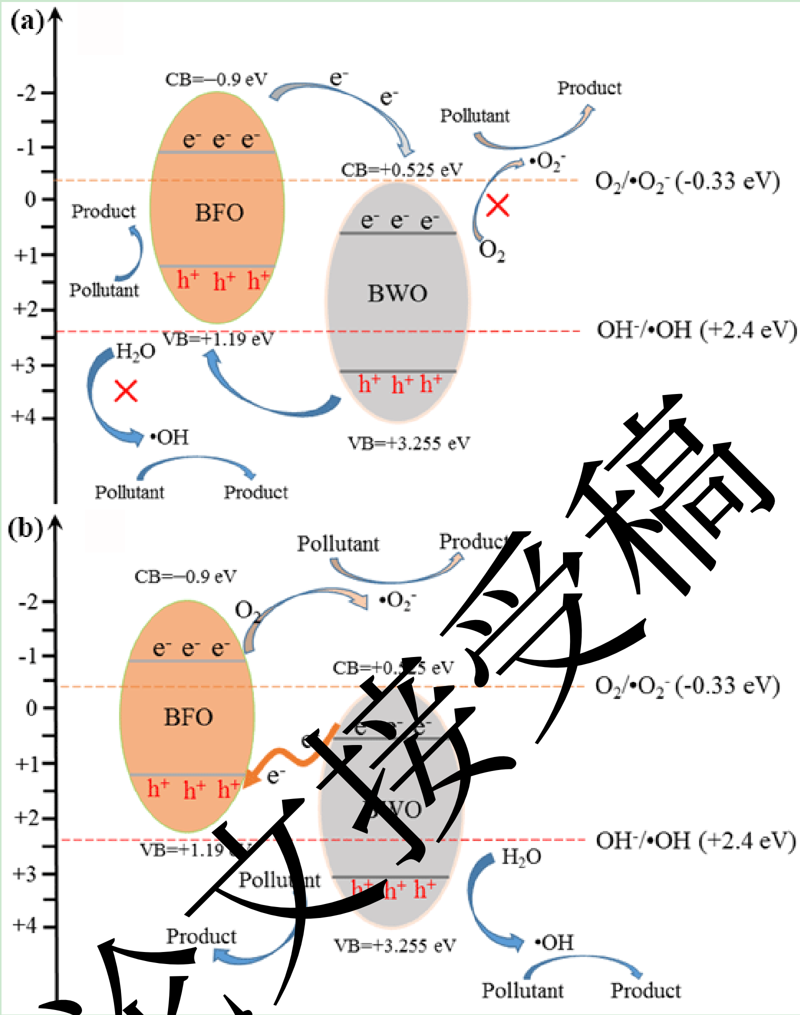

Fig. 8 Proposed mechanism for charge transfer and photocatalytic reaction of the BFWO heterojunction photocatalyst under visible light irradiation: (a) traditional mode and (b) Z-Scheme heterojunction system. Reprinted from ref [93] with permission from The American Chemical Society.

4. Environmental application of nano-structured BWO

The photocatalytic efficiency over BWO is closely correlated with the generation of photoexcited electron-hole pairs and the separation of charge carriers [94]. Additionally, controllable morphology has a significant impact on the optical properties owing to the ability to tune the electronic structure [95-97]. In the past decade, great attention has been paid to tuning the nanostructure of BWO to enhance the photocatalytic performance. Each structure and morphology has its own characteristic depending on the applied conditions. For example, 2D monolayer BWO reveals higher photocatalytic performance if considering the fast migration of charge carriers, while 3D BWO is better for practical application owing to the benefits in efficient separation. Herein, we mainly review the recent applications of modified nano-structured BWO photocatalysts (Table 2), along with exploring the role of active radicals play in the photocatalytic process.

4.1 Application in environmental pollutant treatment

Photoexcited electrons (e^-) in CB and holes (h^+) in VB of nano-structured BWO play an important role in photocatalysis for environmental application [98]. CB e^- can play a direct role in the reduction of inorganic pollutants like bromate, or react with dissolved molecular oxygen for the producation of superoxide radical species to take part in the oxidation of organic pollutants [99, 100]. VB h^+ possess strong oxidation characteristics, which can directly participate in the oxidation of environmental pollutants or react with hydrone for the generation of hydroxyl radical [101-103].

4.1.1 Oxidation of organic pollutants

(i) Colorful dyes. Huge amounts of colourful dyes from dyeing, printing and some other industries widely exist in water resource, which caused a serious water pollution and received worldwide attention. Nano-structured BWO photocatalysts have been proven to reveal excellent catalytic activity in the photodegradation of organic dyes [104-106]. And different from colourless organic and inorganic pollutants, beside photocatalytic process, colourful dyes can be degraded via photolysis or photosensitization [107]. In the photolysis, photoexcited e^- in the dye can react with dissolved oxygen to generate singlet oxygen atom to participate in the oxidation. As for the photosensitization process, photo-electrons can be generated on the dye after being simulated by light irradiation, transferring to CB of nano-structured BWO and then reacting with oxygen to form $\bullet O_2^-$ to participate in the oxidation reaction.

A reduced graphene oxide (RGO)/BWO photocatalyst was used for organic dyes degradation (Fig. 9) [108]. RGO is a strictly zero band gap semi-metal with superior conductivity and adsorptivity, which have an impact on the electronic properties of photocatalysts [109]. More important, some peculiar electronic properties, - such as ambipolar electric field effect, electronic transport via relativistic Dirac fermions and the quantum Hall effect - were observed [110]. Therefore, introduction of RGO can improve the catalytic activity of nano-structured BWO photocatalysts. The enhanced photoactivity is not directly correlated with the band gap, because the introduction of RGO cannot change the band gap of BWO. And using graphene oxide as precursors in the synthesis process might alter the interfacial interactions between RGO and BWO.

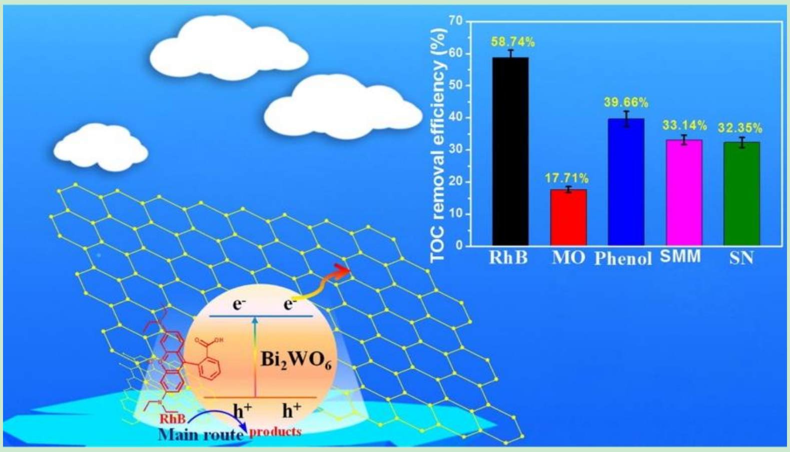

Fig. 9 Proposed mechanism for the transfer of photogenerated charges in the RGO/BWO composites and the photodegradation efficiency of dyes. Reprinted from ref [108] with permission from Elsevier.

(ii) Colorless organics. A mass of organic pollutants are released daily to environment, and many of these pollutants are non-biodegradable, which finally accumulate in living beings and then cause damages [111-113]. Recently, our team utilized a 0D/2D interface engineering of carbon quantum dots (CQDs) modified 2D m-BWO (CBW) to further improve the photocatalytic activity with full spectrum light utilization [114]. 2D m-BWO shows high oxidation efficiency on organic pollutants owing to the improved separation efficiency of electron-hole pairs and solar energy conversion [115]. The as-prepared 0D/2D nano-structured CBW photocatalysts have several advantages: (i) the accessible area between the CQDs and 2D m-BWO interface and the pathways for e^- transfer are well constructed; (ii) wider spectrum of solar can be utilized; (iii) the interfacial charge transfer process can be accelerated because of the more close contact between smaller nano structured photocatalysts and organic pollutants; (iv) the adsorption capacity is enhanced because of the introduction of CQDs sp^2 carbon clusters. CQDs firstly absorbed near-infrared light and emit shorter visible light, leading to up conversion to turn excited m-BWO (Fig. 10a) [114]. And CQDs played as electron acceptors for trapping photogenerated e^- to separate the electron-hole pairs, and the electrons accumulated at a higher energy level in m-BWO, which migrated to the CQDs to generate $\cdot O_2^-$ radicals (Fig. 10b) [114]. The results of photocatalytic degradation experiments showed that CBW revealed excellent photocatalytic oxidation ability on bisphenol A (BPA) owing to the generated ·OH, $\cdot O_2^-$, and h^+ radicals under full spectrum light irradiation.

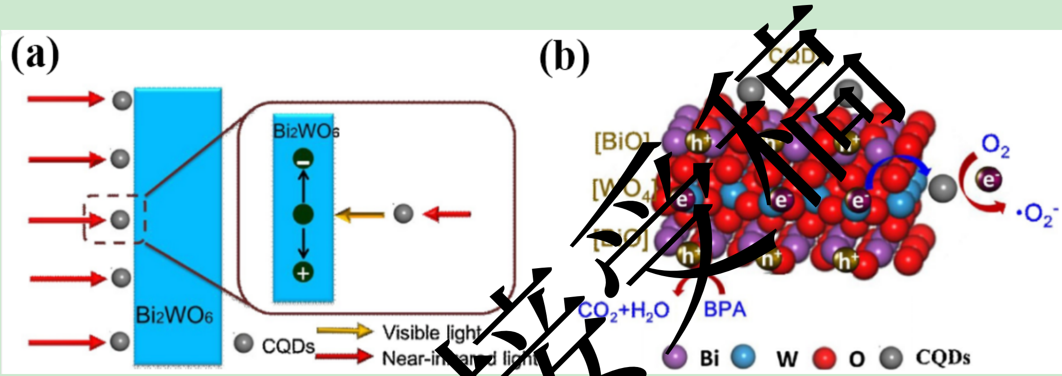

Fig. 10 (a) Schematic diagram for up-converted PL of CBW heterojunctions; (b) photocatalytic mechanism scheme of CBW under full spectrum light irradiation. Reprinted from ref [114] with permission from Elsevier.

Besides, Yao et.al [89] presented a self-assembled perylene diimide (PDI) based supramolecular heterojunction with BWO for photocatalytic degradation of phenol. The BWO/PDI heterojunction was fabricated via thermal treatment, simultaneously PDI self-assembly was finished. The obtained n-n type inorganic-organic heterojunction benefitted the photocatalytic process, because the e^- in the LUMO orbit of PDI were transferred to BWO CB to produce superoxide radicals, which inhibited the recombination of photogenerated charge carriers (Fig. 11) [89]. According to the experimental results, BWO/PDI heterojunction showed higher photocatalytic degradation efficiency on phenol compared with pure BWO.

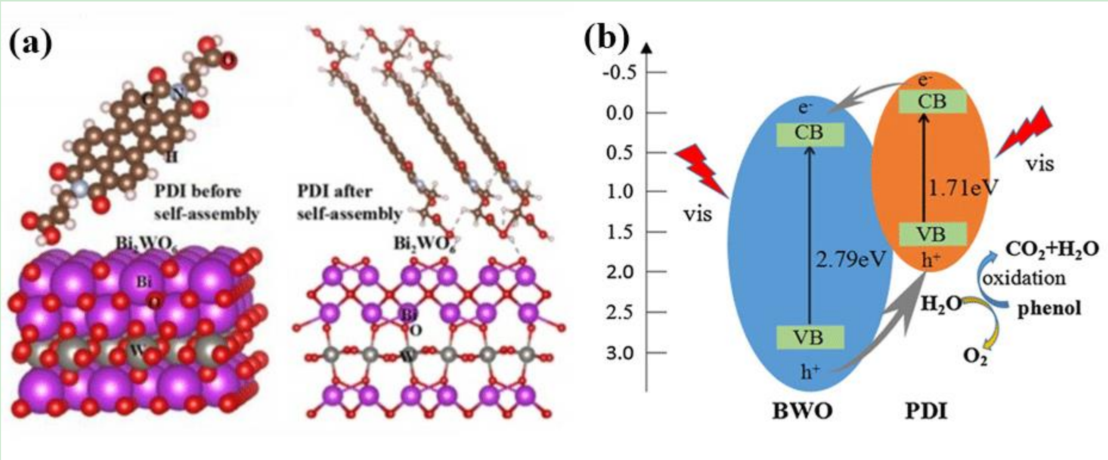

Fig. 11 (a) Self-assembled BWO/PDI heterojunction; (b) Possible reaction mechanism of phenol photodegradation over BWO/PDI heterojunction under visible light. Reprinted from ref [89] with permission from Elsevier.

And in recent years, selective photocatalytic oxidation of organics has also attracted wide attention, which is an environmentally benign way for value-added chemical synthesis [116-120]. BWO was proven to be a highly chemoselective visible light photocatalyst toward the oxidation of benzylic alcohols [121]. The benzylic alcohols were selectively oxidized by photogenerated h^+ and $\cdot O_2^-$ to be corresponding aldehydes over flower-like BWO. This was mainly contributed to the absence of ·OH radicals, slight oxidation ability and stronger adsorption on benzylic alcohols than aldehydes [121]. Lately, Chen et.al [122] presented a 3D hierarchical heterostructure of BWO/$CdWO_4$ (BCW) for selective photocatalytic benzene hydroxylation to phenol with using O_2 as the oxidant. This hierarchical heterostructure showed high photocatalytic performance owing to the improved photoabsorption and charge carriers separation. It was found that ·OH played a pivotal role in the benzene hydroxylation process (Fig. 12) [122].

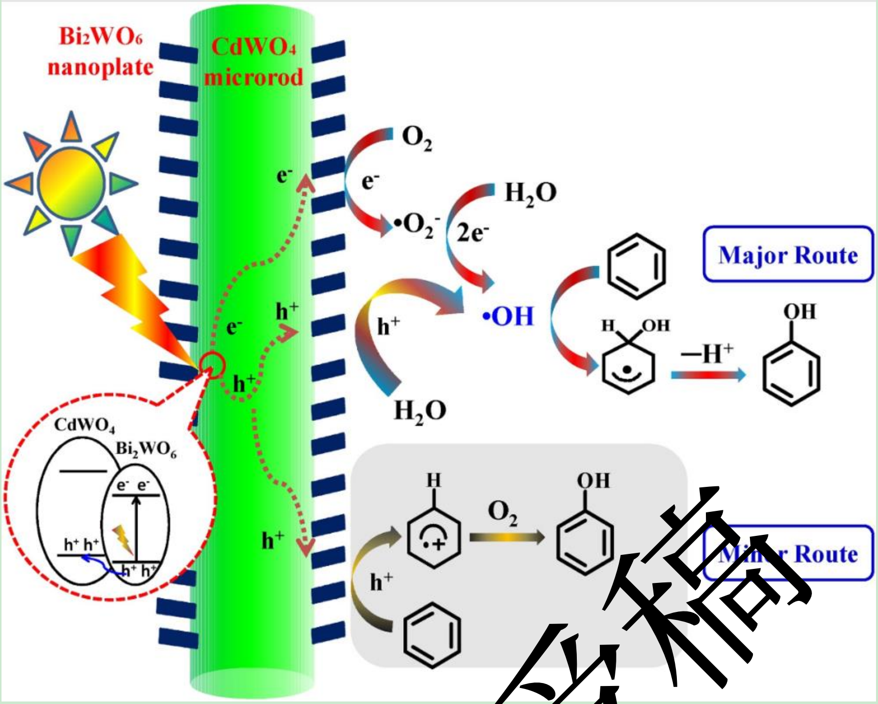

Fig. 12 Proposed mechanism of selective photocatalytic benzene hydroxylation to phenol over BWO/$CdWO_4$. Reprinted from ref. [122] with permission from Elsevier.

4.1.2 Treatment of inorganics

Inorganic pollutants are non-biodegradable, like nitric oxides (NO_x), bromate and heavy metal ions, which are dangerous for biological bodies when they accumulate to a certain amount [123, 124]. Photocatalytic process over nano-structured BWO is alternative for the treatment of the inorganic pollutants. For example, graphene (GR)/BWO composites was used for the photocatalytic oxidation of NO because the introduction of GR contributed to a positive shift of the Fermi level [125]. And very recently, Fan et al. [126] presented a mesoporous nanoplate multi-directional assembled BWO architecture (BWO-180-C) for oxidation of NO (Fig. 13). Beside the exposed crystal faces, crystallinity, photoabsorption and charge carriers separation, mass transfer and interconnected porous networks with appropriate pores size have a significant impact on the optical properties and catalytic performance of hierarchically structured mesoporous BWO in NO oxidation.

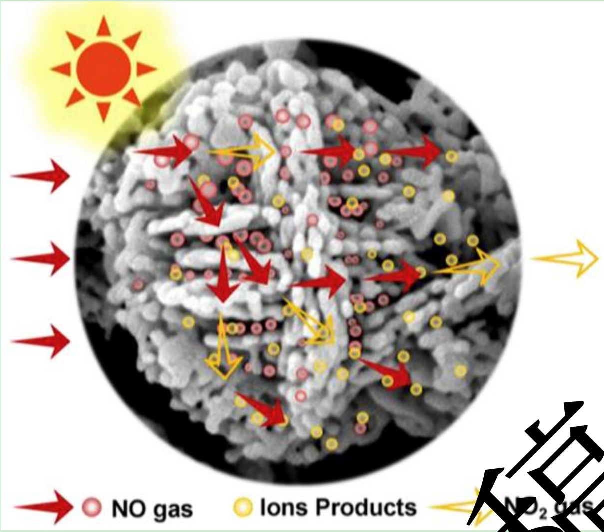

Fig. 13 Diffusion of NO over mesoporous nanoplate multi-directional assembled BWO. Reprinted from ref [126] with permission from Elsevier.

Beside photocatalytic oxidation performance, nano-structured BWO shows high photocatalytic reduction activity for inorganic pollutant, like highly-toxic heavy metal ions chromium (Cr). Reduction of Cr(VI) to Cr(III) is a conventional treatment method, because the toxicity of Cr(III) is found to be much less than that of Cr(VI) [127-129]. Guo et al. [130] prepared an oxygen vacant CeO_2@BWO hollow magnetic microcapsule heterostructure for higher photocatalytic activity for Cr(VI) reduction (Fig. 14). On the one hand, the oxygen vacancy and heterostructure can enhance the charge carriers separation and interfacial charge transfer efficiency. On the other hand, the hollow microcapsule can improve the light efficiency because of the multiple reflections. The results showed that the obtained CeO_2@BWO composites could completely absorb Cr(III), and it is easy for the composites to be recovered and reutilized owing to the magnetic property [130].

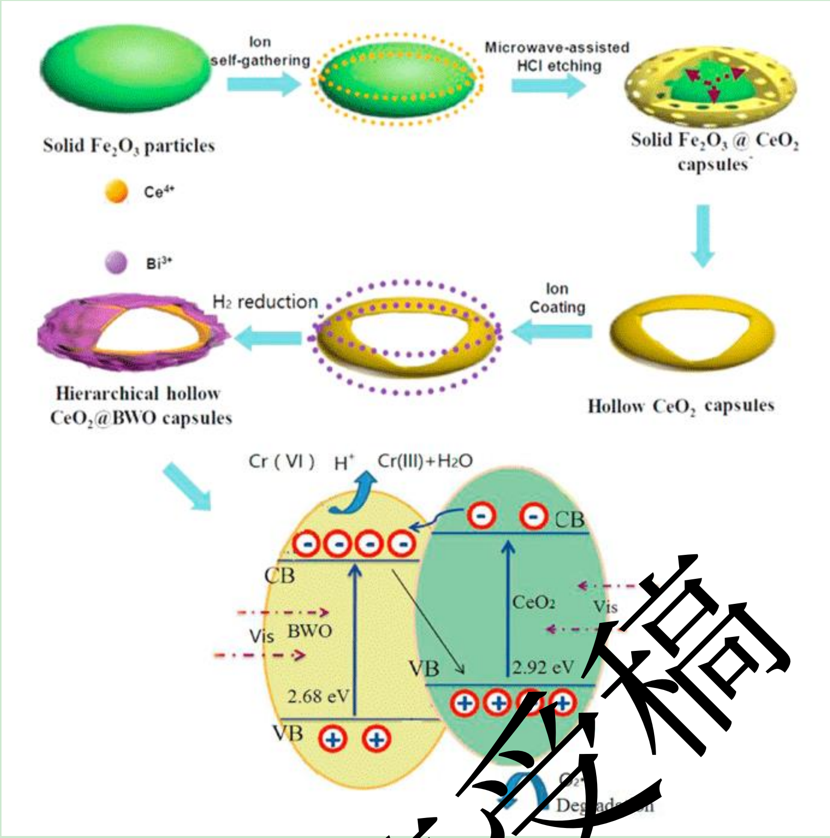

Fig. 14 The assemble process and photogenerated charge carriers transfer of CeO_2@BWO. Reprinted from ref. [130] with permission from Elsevier.

4.2 Application in clean-energy production

4.2.1 Fuel energy production

Photocatalytic process is the common method used for CO_2 reduction [131]. Many semiconductor materials have been studied to be electrocatalysts or photocatalysts since CO_2 was reduced to methane, formaldehyde, and methyl alcohol via a photoelectrocatalytic process with photosensitive semiconductors as catalysts [132-134]. In recent years, BWO has been one of the most widely investigated CO_2 photoreduction catalysts [135].And an ultrathin BWO square nanoplate with ~9.5 nm thickness showed the capacity to utilize solar light energy for reducing CO_2 into hydrocarbon fuel [136]. The ultrathin geometry allows a rapid transportation of photogenerated e^- from the interior to the surface and accelerates the separation of photoexcited e^-- h^+ pairs [136].

However, few pure nano-structured BWO semiconductors have the ability to transfer a single photogenerated electron to carbon dioxide. A proton-assisted transfer of multiple electrons was used for easier CO_2 photoreduction process. And the atomically-thin oxide-based semiconductor was an excellent platform for solar CO_2 reduction. Therefore, a prototype single-unit-cell BWO layers were prepared successfully through a lamellar Bi-oleate intermediate [38]. Atomically-thin oxide-based BWO can provide abundant catalytically active sites, enhanced 2D conductivity, and remarkable structural stability. Owing to the unique geometric structure, the single-unit-cell BWO layers revealed high adsorption of CO_2. Additionally, the increased conductivity accelerated carrier transport, leading to the improved separation of e^-- h^+ pairs. And according to the UV/Vis diffuse reflectance spectra analysis, the single-unit-cell BWO layers showed higher efficiency of light absorption (Fig. 15) [38]. These accounted for the improved photocatalytic performance on the reduction of CO_2.

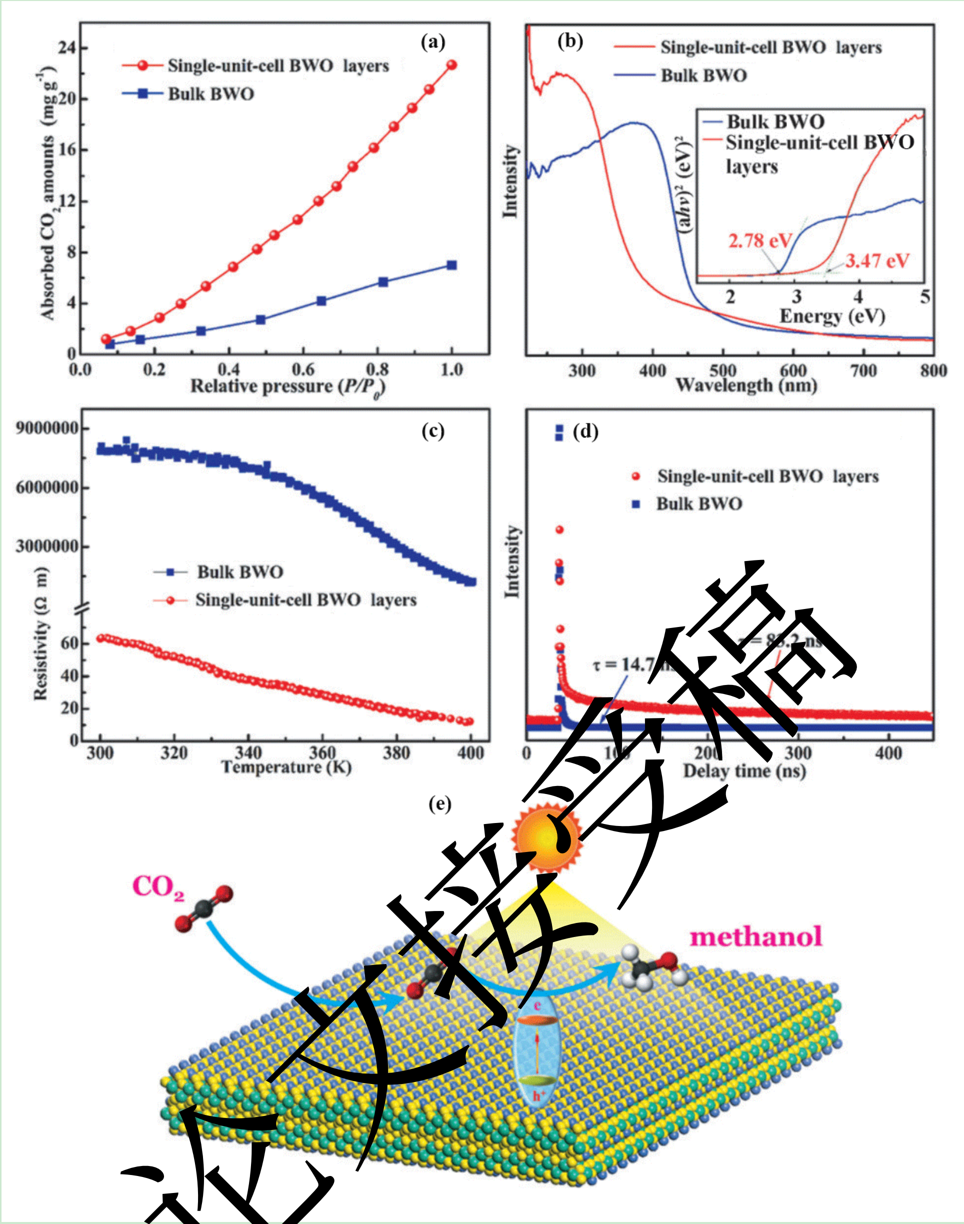

Fig. 15 (a) CO_2 adsorption isotherms, (b) UV/Vis diffuse reflectance spectra, (c) temperature-dependent resistivity, and (d) fluorescence emission decay spectra of single-unit-cell BWO layers and bulk BWO; (e) illustration of the photocatalytic reduction of CO_2 over single-unit-cell BWO layers. Reprinted from ref [38] with permission from Wiley.

Besides, graphitic carbon nitride (g-C_3N_4) was used to couple with BWO to form a novel photocatalyst for CO_2 reduction [137]. 2D g-C_3N_4 can absorb visible and near-infrared light with a band gap of 2.7 eV. The g-C_3N_4/BWO composites were synthesized through a hydrothermal method: (i) thermally decomposing urea at 550 ℃ for 2 h in static air to get metal-free g-C_3N_4; (ii) mixing $Na_2WO_4 \cdot 2H_2O$ and g-C_3N_4 into deionized water with a ultrasound treatment; (iii) adding $Bi(NO_3)_3 \cdot 5H_2O$ to HNO_3 to form a solution, then dropping the $Na_2WO_4 \cdot 2H_2O$ and g-C3N4 mixture to this solution under strong stirring; (iv) adding oleyl amine and $NH_3 \cdot H_2O$ into the above mixture; (v) the final mixture was transferred into a Teflon-lined autoclave with heating at 200 ℃ for 20 h. The enhanced photoreduction of CO_2 was contributed to the accelerated transport of charge carriers and improved separation of photogenerated e^--h^+ pairs (Fig. 16). Under light irradiation, g-C_3N_4/BWO produced photoexcited electron-hole pairs with electrons transferred to CB of BWO and the holes remained in VB of g-C_3N_4. H_2O was oxidized via holes at VB of g-C_3N_4 to produce O_2 and protons, while CO_2 was reduced to CO via electrons at CB of BWO with the assistance of protons generated at VB of g-C_3N_4.

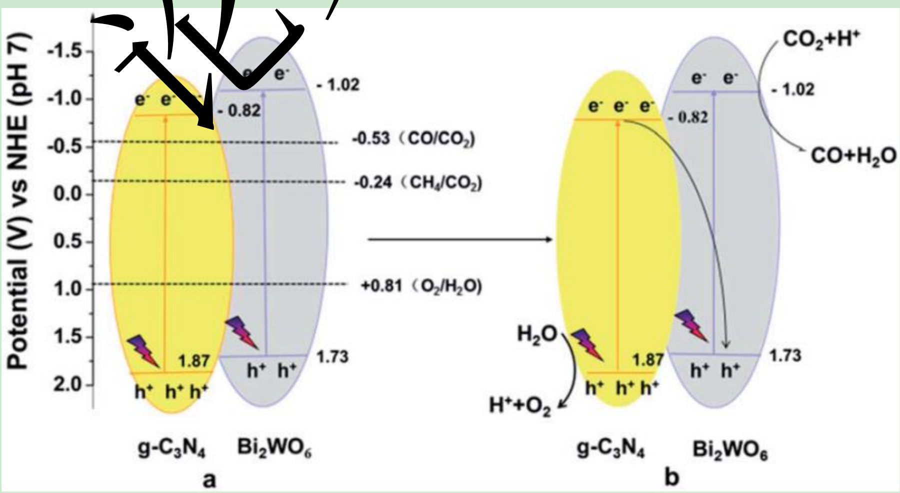

Fig. 16 (a) Presented mechanism in the heterostructure: electron and hole pairs generated in g-C_3N_4 and BWO under visible light irradiation; (b) the electrons in CB of

$g-C_3N_4$ migrate to VB of BWO. Adapted from ref [137] with permission from The Royal Society of Chemistry.

4.2.2 Hydrogen production

Nano-structured BWO photocatalysts show great potential in hydrogen production via solar water-splitting process [138-141]. Photoexcited electrons are the major substances in hydrogen production process, and condcution band energy level of modified nano-structured BWO is required to be more negative than hydrogen evolution level. Today, heterojunction construction is an alternative method to enhance the catalytic activity of nano-structured BWO photocatalysts in hydrogen production. Conventional heterostructure can improve the sepration of photoexcited e^{-}- h^{+} pairs, but the redox range is still narrow [122]. Therefore, more and more novel heterostructures have been designed for higher hydrogen production. Recently, a mediator- and co-catalyst-free direct Z-scheme compsite of BWO-Cu_3P was designed for more efficient photocatalytic water-splitting to produce hygrogen [142]. The BWO-Cu_3P composite was prepared via a straightforward ball-milling complexation method. In this Z-scheme system composed of BWO-Cu_3P, the well-balanced position of energy levels play an improtant role in the improvement of the photocatalytic activity. A possible mechanism of solar-water splitting over BWO-Cu_3P composite were presented based on the energy levels position of BWO and Cu_3P (Fig. 17) [142]. Compared with conventional heterostructures, the charge transfer pathway of Z-scheme-based BWO-Cu_3P is different, and the redox range becomes wider [142].

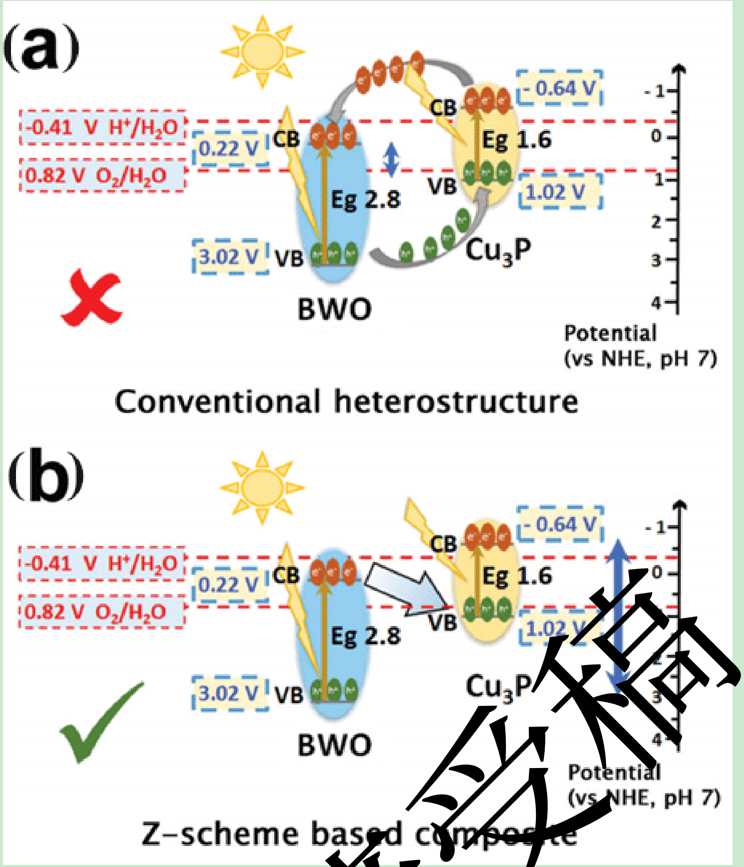

Fig. 17 Charge transfer pathway of (a) conventional heterostructure and (b) Z-scheme-based BWO-Cu_3P photocatalyst. Reprinted from ref [142] with permission from The Royal Society of Chemistry.

5. Summary and prospects

5.1 Summary

In this review, we sum up the recent development of nano-structured BWO with controllable morphology, including fabrication for different dimensional structures, modification methods of nano-structured BWO to improve the photocatalytic performance, and advanced application in environmental pollutant treatment and clean-energy production. Various morphological BWO crystals have been prepared successfully on a large scale through various methods. The continuing breakthroughs in the controllable fabrication and modification ways nano-structured BWO photocatalysts have brought different size, shapes, surface areas, light absorption ranges, and energy band structures. Correspondingly, the photocatalytic properties and performance were different. Nano-structured BWO photocatalysts play a significant role in addressing the environmental issues, including environmental pollution and clean-energy shortage.

Since the photocatalytic performances of nano-structured BWO photocatalysts are mainly affected by their light-responsive range and carrier-separation ability, rational design on their structure and chemical connection meeting the requirement is important. For example, 3D nano-scale hierarchical structures of BWO assemblies, - such as flower-like or flake ball-shaped structure, hierarchical microsphere, nano-structured particles with porous nanoplates, and porous hollow structure, - merit wide attention owing to the superstructure benefits the photocatalytic process and recycling process of BWO. And compared with 3D nano structures, 2D nano-structured BWO are believed to perform better in photogenerated charge carriers separation. This is because the photogenerated electron-hole pairs in 2D structure can come up to the surface more quickly than that produced deeply in 3D structure. Different from 3D and 2D nano structures, 1D nano-structured BWO exhibit obvious chemical and structural behaviour owing to the remarkable length-to-diameter ratio and exclusive two-dimensional confinement.

For pure nano-structured BWO applied in photocatalytic process, high recombination of photogenerated electron-hole pairs and narrow photoabsorption range are the major limitations. Hence, modification methods were further explored to enlarge the photocatalytic application of BWO, including morphological manipulation, structure modification through doping or substitution, solid solution fabrication, and compound formation. Besides, coating with electroconductive materials (like carbon materials) [143-145] and synergetic effect via photoelectrocatalytic process [146-148] are efficient ways to enhance the photocatalytic activity of nano-structured BWO. So far, much attention has been paid to make full use of the structure- and morphology-dependent properties of different dimensional BWO. However, research on the optimization of photocatalytic properties of different dimensional nano-structured BWO are still in their infancy. A further comprehensive exploration on the factors governing the photocatalytic activity of nano-structured BWO photocatalysts with controlled morphology are in demand.

In spite of the young research on the optimization of photocatalytic properties, nano structures of BWO hold wonderful potential to solve the environmental issues. Nano-structured BWO with controlled morphology are believed to be more applicable in environmental pollutant treatment and clean-energy production, eventually being applied in wider fields. With the development of nanotechnology, multiple opportunities will emerge to advance nano-structured BWO photocatalysts into a powerful tool to be applied in environment beyond we have realized to date.

5.2 Challenges and prospects

The promising opportunities provided by controllable fabrication of BWO are brilliant. Simultaneously, challenges exist together with opportunities, which are waiting to be resolved.

(i) In structure fabrication, ordered growth of electroconductive materials on layered BWO to avoid the loss of active sites and cost reduce in preparation and recycling process for commercial application are the main challenges.

(ii) When nano-structured BWO are applied in our life for pollutant treatment and clean-energy production, most of them will become deposition into water or soil environment. Such deposited BWO in water could produce toxicity to living cells via the generated reactive oxygen and radicals (Fig. 18). Research on the toxicity of nano-structured BWO on environmental living cells is still absent.

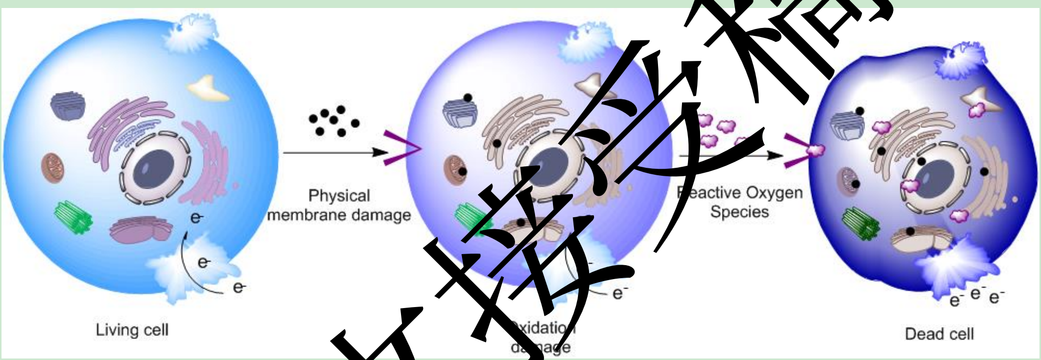

Fig. 18 Major toxicity mechanism of BWO nanostructures on cells.

(iii) For application in the removal of pollutants over nano-structured BWO, most of the researchers centred on a simple kind of environmental pollutant and the application was limited in water environment. But in practical application, numerous pollutants exist in the total environment. Efficient treatment methods for more complex environmental matrix with using nano-structured BWO photocatalysts are in their initial stage.

(iv) For clean-energy production, small reactor is the main limitation, and the output of clean-energy cannot reach the demand of real application. And generally, special trapping agent are needed in the reaction, such as h^+ scavenger or O_2 trapping agent used in hydrogen production, which will increase the cost of whole process.

It is anticipated this review will be a powerful resource to strengthen the efforts to explore simpler methods for controllable fabrication of BWO nano structures with showing excellent photocatalytic performance in environmental application. Reasonable design and full exploration of nano structures and photocatalytic properties can enrich the application of BWO for the utilization of solar energy. We believe that this review will open a wider path with summarizing advanced fabrication approaches, modifications, environmental applications and challenges for further development not only in the catalytic process over BWO photocatalysts but throughout all the catalytic systems.

Acknowledgments

This study was financially supported by the Program for the National Natural Science Foundation of China (51579098, 51779090, 51709101, 51278176, 51408206, 51521006), Science and Technology Plan Project of Hunan Province (2017SK2243, 2016RS3026), the National Program for Support of Top-Notch Young Professionals of China (2014), the Program for New Century Excellent Talents in University (NCET-13-0186), the Program for Changjiang Scholars and Innovative Research Team in University (IRT-13R17), and the Fundamental Research Funds for the Central Universities (531107050978, 531107051080).

References

[1] B. Obama, The irreversible momentum of clean energy, Science 355 (2017) 126-129.

[2] A. Shah, S. Shahzad, A. Munir, M.N. Nadagouda, G.S. Khan, D.F. Shams, D.D. Dionysiou, U.A. Rana, Micelles as Soil and Water Decontamination Agents, Chem. Rev. 116 (2016) 6042-6074.

[3] L. Qin, G. Zeng, C. Lai, D. Huang, P. Xu, C. Zhang, M. Cheng, X. Liu, S. Liu, B. Li, H. Yi, “Gold rush” in modern science: Fabrication strategies and typical advanced applications of gold nanoparticles in sensing, Coord. Chem. Rev. 359 (2018) 1-31.

[4] X. Ren, G. Zeng, L. Tang, J. Wang, J. Wan, Y. Liu, J. Yu, H. Yi, S. Ye, R. Deng, Sorption, transport and biodegradation - An insight into bioavailability of persistent organic pollutants in soil, Sci. Total Environ. 610-611 (2018) 1154-1163.

[5] P. Xu, G.M. Zeng, D.L. Huang, C.L. Feng, S. Hu, M.H. Zhao, C. Lai, Z. Wei, C. Huang, G.X. Xie, Z.F. Liu, Use of iron oxide nanomaterials in wastewater treatment: A review, Sci. Total Environ. 424 (2012) 1-10.

[6] J. Gong, B. Wang, G. Zeng, C. Yang, C. Niu, Q. Niu, W. Zhou, Y. Liang, Removal of cationic dyes from aqueous solution using magnetic multi-wall carbon nanotube nanocomposite as adsorbent, J. Hazard. Mater. 164 (2009) 1517-1522.

[7] C. Lai, X. Liu, L. Qin, C. Zhang, G. Zeng, D. Huang, M. Cheng, P. Xu, H. Yi, D. Huang, Chitosan-wrapped gold nanoparticles for hydrogen-bonding recognition and colorimetric determination of the antibiotic kanamycin, Microchim. Acta 184 (2017) 2097-2105.

[8] L. Qin, G. Zeng, C. Lai, D. Huang, C. Zhang, P. Xu, T. Hu, X. Liu, M. Cheng, Y. Liu, L. Hu, Y. Zhou, A visual application of gold nanoparticles: Simple, reliable and sensitive detection of kanamycin based on hydrogen-bonding recognition, Sens. Actuators, B: Chem. 243 (2017) 946-954.

[9] H. Wu, C. Lai, G. Zeng, J. Liang, J. Chen, J. Xu, J. Dai, X. Li, J. Liu, M. Chen, L. Lu, L. Hu, J. Wan, The interactions of composting and biochar and their implications for soil amendment and pollution remediation: a review, Crit. Rev. Biotechnol. 37 (2017) 754-764.

[10] X. Gong, D. Huang, Y. Liu, G. Zeng, R. Wang, J. Wan, C. Zhang, M. Cheng, X. Qin, W. Xue, Stabilized nanoscale zerovalent iron mediated cadmium accumulation and oxidative damage of Boehmeria nivea (L.) Gaudich cultivated in cadmium contaminated sediments, Environ. Sci. Technol. 51 (2017) 11308-11316.

[11] C. Ming, P. Xu, G. Zeng, C. Yang, D. Huang, J. Zhang, Bioremediation of soils contaminated with polycyclic aromatic hydrocarbons, petroleum, pesticides, chlorophenols and heavy metals by composting: Applications, microbes and future research needs, Biotechnol. Adv. 33 (2015) 745-755.

[12] Y. Zhang, G.M. Zeng, L. Tang, J. Chen, Y. Zhu, X.X. He, Y. He, Electrochemical sensor based on electrodeposited graphene-Au modified electrode and nanoAu carrier amplified signal strategy for attomolar mercury detection, Anal. Chem. 87 (2015) 989-996.

[13] M. Cheng, G. Zeng, D. Huang, C. Lai, P. Xu, C. Zhang, Y. Liu, Hydroxyl radicals

based advanced oxidation processes (AOPs) for remediation of soils contaminated with organic compounds: A review, Chem. Eng. J. 284 (2016) 582-598.
[14] C.Y. Zhu, G.D. Fang, D.D. Dionysiou, C. Liu, J. Gao, W.X. Qin, D.M. Zhou, Efficient transformation of DDTs with Persulfate Activation by Zero-valent Iron Nanoparticles: A Mechanistic Study, J. Hazard. Mater. 316 (2016) 232-241.
[15] F. Long, J.-L. Gong, G.-M. Zeng, L. Chen, X.-Y. Wang, J.-H. Deng, Q.-Y. Niu, H.-Y. Zhang, X.-R. Zhang, Removal of phosphate from aqueous solution by magnetic Fe–Zr binary oxide, Chem. Eng. J. 171 (2011) 448-455.
[16] J. Liang, Z. Yang, L. Tang, G. Zeng, M. Yu, X. Li, H. Wu, Y. Qian, X. Li, Y. Luo, Changes in heavy metal mobility and availability from contaminated wetland soil remediated with combined biochar-compost, Chemosphere 181 (2017) 281-288.
[17] J.-H. Deng, X.-R. Zhang, G.-M. Zeng, J.-L. Gong, Q.-Y. Niu, J. Liang, Simultaneous removal of Cd(II) and ionic dyes from aqueous solution using magnetic graphene oxide nanocomposite as an adsorbent, Chem. Eng. J. 226 (2013) 189-200.
[18] P. Xu, G.M. Zeng, D.L. Huang, C. Lai, M.H. Zhao, Z. Wei, N.J. Li, C. Huang, G.X. Xie, Adsorption of Pb(II) by iron oxide nanoparticles immobilized Phanerochaete chrysosporium: Equilibrium, kinetic, thermodynamic and mechanisms analysis, Chem. Eng. J. 203 (2012) 423-431.
[19] H. Yi, G. Zeng, C. Lai, D. Huang, L. Tang, J. Gong, M. Chen, P. Xu, H. Wang, M. Cheng, C. Zhang, W. Xiong, Environment-friendly fullerene separation methods, Chem. Eng. J. 330 (2017) 134-145.
[20] C. Zhang, C. Lai, G. Zeng, D. Huang, C. Yang, Y. Wang, Y. Zhou, M. Cheng, Efficacy of carbonaceous nanocomposites for sorbing ionizable antibiotic sulfamethazine from aqueous solution, Water Res. 95 (2016) 103-112.
[21] W.-W. Tang, G.-M. Zeng, J.-L. Gong, J. Liang, P. Xu, C. Zhang, B.-B. Huang, Impact of humic/fulvic acid on the removal of heavy metals from aqueous solutions using nanomaterials: a review, Sci. Total Environ. 468 (2014) 1014-1027.
[22] J. Di, C. Yan, A.D. Handoko, Z.W. Seh, H. Li, Z. Liu, Ultrathin two-dimensional materials for photo- and electrocatalytic hydrogen evolution, Mater. Today 21 (2018) 749-770.
[23] L. Tang, Y. Liu, J. Wang, G. Zeng, Y. Deng, H. Dong, H. Feng, J. Wang, B. Peng, Enhanced activation process of persulfate by mesoporous carbon for degradation of aqueous organic pollutants: Electron transfer mechanism, Appl. Catal. B: Environ. 231 (2018) 1-10.
[24] Y. Lin, S. Wu, X. Li, X. Wu, C. Yang, G. Zeng, Y. Peng, Q. Zhou, L. Lu, Microstructure and performance of Z-scheme photocatalyst of silver phosphate modified by MWCNTs and Cr-doped $SrTiO_3$ for malachite green degradation, Appl. Catal. B: Environ. 227 (2018) 557-570.
[25] H. Wang, Y. Wu, X.Z. Yuan, G.M. Zeng, J. Zhou, X. Wang, J.W. Chew, Clay-Inspired MXene-Based Electrochemical Devices and Photo-Electrocatalyst: State-of-the-Art Progresses and Challenges, Adv. Mater. 30 (2018) 1704561.
[26] C. Zhou, C. Lai, D. Huang, G. Zeng, C. Zhang, M. Cheng, L. Hu, J. Wan, W. Xiong, M. Wen, X. Wen, L. Qin, Highly porous carbon nitride by supramolecular preassembly of monomers for photocatalytic removal of sulfamethazine under visible

light driven, Appl. Catal. B: Environ. 220 (2018) 202-210.
[27] X. Zhou, C. Lai, D. Huang, G. Zeng, L. Chen, L. Qin, P. Xu, M. Cheng, C. Huang, C. Zhang, C. Zhou, Preparation of water-compatible molecularly imprinted thiol-functionalized activated titanium dioxide: Selective adsorption and efficient photodegradation of 2, 4-dinitrophenol in aqueous solution, J. Hazard. Mater. 346 (2018) 113-123.
[28] H. Wang, X. Yuan, H. Wang, X. Chen, Z. Wu, L. Jiang, W. Xiong, G. Zeng, Facile synthesis of Sb_2S_3/ultrathin g-C_3N_4 sheets heterostructures embedded with g-C_3N_4 quantum dots with enhanced NIR-light photocatalytic performance, Appl. Catal. B: Environ. 193 (2016) 36-46.
[29] C. Lai, M.-M. Wang, G.-M. Zeng, Y.-G. Liu, D.-L. Huang, C. Zhang, R.-Z. Wang, P. Xu, M. Cheng, C. Huang, Synthesis of surface molecular imprinted TiO_2/graphene photocatalyst and its highly efficient photocatalytic degradation of target pollutant under visible light irradiation, Appl. Surf. Sci. 390 (2016) 368-376.
[30] C.Q. Lia, Z.M. Sun, A.K. Song, X.B. Dong, S.L. Zheng, D.D. Dionysiou, Flowing nitrogen atmosphere induced rich oxygen vacancies overspread the surface of TiO_2/kaolinite composite for enhanced photocatalytic activity within broad radiation spectrum, Appl. Catal. B: Environ. 236 (2018) 76-87.
[31] X.L. Ma, H. Li, T.Y. Liu, S.S. Du, Q.P. Qiang, Y.H. Wang, S. Yin, T. Sato, Comparison of photocatalytic reaction-induced selective corrosion with photocorrosion: Impact on morphology and stability of Ag-ZnO, Appl. Catal. B: Environ. 201 (2017) 348-358.
[32] D. Adak, B. Show, A. Mondal, N. Mukherjee, ZnO/γ-Fe_2O_3 charge transfer interface in zinc-iron oxide hollow cages towards efficient photodegradation of industrial dyes and methanol electrooxidation, J. Catal. 355 (2017) 63-72.
[33] C. Liu, C. Cao, X. Luo, S. Luo, Ag-bridged Ag_2O nanowire network/TiO_2 nanotube array p–n heterojunction as a highly efficient and stable visible light photocatalyst, J. Hazard. Mater. 285 (2015) 319-324.
[34] C. Zhou, C. Lai, P. Xu, G. Zeng, D. Huang, C. Zhang, M. Cheng, L. Hu, J. Wan, Y. Liu, W. Xiong, Y. Deng, M. Wen, In Situ Grown AgI/$Bi_{12}O_{17}Cl_2$ Heterojunction Photocatalysts for Visible Light Degradation of Sulfamethazine: Efficiency, Pathway, and Mechanism, ACS Sustain. Chem. Eng. 6 (2018) 4174-4184.
[35] C.L. Yu, Z. Wu, R.Y. Liu, D.D. Dionysiou, K. Yang, C.Y. Wang, H. Liu, Novel fluorinated Bi_2MoO_6 nanocrystals for efficient photocatalytic removal of water organic pollutants under different light source illumination, Appl. Catal. B: Environ. 209 (2017) 1-11.
[36] S. Song, H. Yang, C.L. Zhou, J. Cheng, Z.B. Jiang, Z. Lu, J. Miao, Underwater superoleophobic mesh based on $BiVO_4$ nanoparticles with sunlight-driven self-cleaning property for oil/water separation, Chem. Eng. J. 320 (2017) 342-351.
[37] J. Hou, S. Cao, Y. Wu, F. Liang, Y. Sun, Z. Lin, L. Sun, Simultaneously efficient light absorption and charge transport of phosphate and oxygen-vacancy confined in bismuth tungstate atomic layers triggering robust solar CO_2 reduction, Nano Energy 32 (2017) 359-366.
[38] L. Liang, F. Lei, S. Gao, Y. Sun, X. Jiao, J. Wu, S. Qamar, Y. Xie, Single Unit

Cell Bismuth Tungstate Layers Realizing Robust Solar CO_2 Reduction to Methanol, Angew. Chem. Int. Ed. 54 (2015) 13971-13974.
[39] N. Zhang, R. Ciriminna, M. Pagliaro, Y.J. Xu, Nanochemistry-derived Bi_2WO_6 nanostructures: towards production of sustainable chemicals and fuels induced by visible light, Chem. Soc. Rev. 43 (2014) 5276-5287.
[40] S.H. Chen, Z. Yin, S.L. Luo, X.J. Li, L.X. Yang, F. Deng, Photoreactive mesoporous carbon/Bi_2WO_6 composites: Synthesis and reactivity, Appl. Surf. Sci. 259 (2012) 7-12.
[41] A. Kudo, S. Hijii, H_2 or O_2 Evolution from Aqueous Solutions on Layered Oxide Photocatalysts Consisting of Bi^{3+} with $6s^2$ Configuration and d^0 Transition Metal Ions, Chem. Lett. 28 (1999) 1103-1104.
[42] C.L. Yu, W.Q. Zhou, H. Liu, Y. Liu, D.D. Dionysiou, Design and fabrication of microsphere photocatalysts for environmental purification and energy conversion, Chem. Eng. J. 287 (2016) 117-129.
[43] T. Han, X. Wang, Y. Ma, G. Shao, X. Dong, C. Yu, Mesoporous Bi_2WO_6 sheets synthesized via a sol–gel freeze-drying method with excellent photocatalytic performance, J. Sol-Gel Sci. Technol. 82 (2017) 101-108.
[44] A. Kaur, S.K. Kansal, Bi_2WO_6 nanocuboids: An efficient visible light active photocatalyst for the degradation of levofloxacin drug in aqueous phase, Chem. Eng. J. 302 (2016) 194-203.
[45] S.T. Lai, P. Zhang, W.Y. Zhou, Z.H. Xu, Z.H. Yang, Synthesis and Properties of Visible-light Photocatalytic Bi_2WO_6 via Microemulsion-assisted Hydrothermal Method, J. Inorg. Mater. 27 (2012) 945-950.
[46] H. Hori, M. Takase, M. Takashima, F. Amano, T. Shibayama, B. Ohtani, Mechanism of formation, structural characteristics and photocatalytic activities of hierarchical-structured bismuth-tungstate particles, Catal. Today 300 (2018) 99-111.
[47] S.O. Alfaro, A. Martinez-de la Cruz, Synthesis, characterization and visible-light photocatalytic properties of Bi_2WO_6 and $Bi_2W_2O_9$ obtained by co-precipitation method, Appl. Catal. A 383 (2010) 128-133.
[48] L. Zhang, Q. Bai, K. Jin, L. Wang, Y. Zhang, S. Yanhua, Synthesis and electrochemical performance of Bi_2WO_6/graphene composite as anode material for lithium-ion batteries, Mater. Lett. 141 (2015) 88-91.
[49] Y.N. Su, G.Q. Tan, T. Liu, L. Lv, Y. Wang, X.L. Zhang, Z.W. Yue, H.J. Ren, A. Xia, Photocatalytic properties of Bi_2WO_6/$BiPO_4$ Z-scheme photocatalysts induced by double internal electric fields, Appl. Surf. Sci. 457 (2018) 104-114.
[50] Y. Zhu, Y. Wang, Q. Ling, Y. Zhu, Enhancement of full-spectrum photocatalytic activity over $BiPO_4$/Bi_2WO_6 composites, Appl. Catal. B: Environ. 200 (2017) 222-229.
[51] Y.H. Xiang, P. Ju, Y. Wang, Y. Sun, D. Zhang, J.Q. Yu, Chemical etching preparation of the Bi_2WO_6/BiOI p-n heterojunction with enhanced photocatalytic antifouling activity under visible light irradiation, Chem. Eng. J. 288 (2016) 264-275.
[52] S.Y. Dong, X.H. Ding, T. Guo, X.P. Yue, X. Han, J.H. Sun, Self-assembled hollow sphere shaped Bi_2WO_6/RGO composites for efficient sunlight-driven photocatalytic degradation of organic pollutants, Chem. Eng. J. 316 (2017) 778-789.

[53] D. Ma, J. Wu, M. Gao, Y. Xin, T. Ma, Y. Sun, Fabrication of Z-scheme g-C_3N_4/RGO/Bi_2WO_6 photocatalyst with enhanced visible-light photocatalytic activity, Chem. Eng. J. 290 (2016) 136-146.
[54] L. Zhang, H. Wang, Z. Chen, P.K. Wong, J. Liu, Bi_2WO_6 micro/nano-structures: Synthesis, modifications and visible-light-driven photocatalytic applications, Appl. Catal. B: Environ. 106 (2011) 1-13.
[55] L. Zhang, Y. Zhu, A review of controllable synthesis and enhancement of performances of bismuth tungstate visible-light-driven photocatalysts, Catal. Sci. Technol. 2 (2012) 694-706.
[56] J.J. Yang, D.M. Chen, Y. Zhu, Y.M. Zhang, Y.F. Zhu, 3D-3D porous Bi_2WO_6/graphene hydrogel composite with excellent synergistic effect of adsorption-enrichment and photocatalytic degradation, Appl. Catal. B: Environ. 205 (2017) 228-237.
[57] X.J. Zhang, S. Yu, Y. Liu, Q. Zhang, Y. Zhou, Photoreduction of non-noble metal Bi on the surface of Bi_2WO_6 for enhanced visible light photocatalysis, Appl. Surf. Sci. 396 (2017) 652-658.
[58] H. Yi, M. Jiang, D. Huang, G. Zeng, C. Lai, L. Qin, C. Zhou, B. Li, X. Liu, M. Cheng, W. Xue, P. Xu, C. Zhang, Advanced photocatalytic Fenton-like process over biomimetic hemin-Bi_2WO_6 with enhanced pH, J. Taiwan Inst. Chem. Eng. (2018).
[59] L. Zhang, W. Wang, Z. Chen, L. Zhou, H. Xu, W. Zhu, Fabrication of flower-like Bi_2WO_6 superstructures as high performance visible-light driven photocatalysts, J. Mater. Chem. 17 (2007) 2526-2532.
[60] Y. Liu, H. Tang, H. Lv, Z. Li, Z. Ding, S. Li, Self-assembled three-dimensional hierarchical Bi_2WO_6 microspheres by sol-gel-hydrothermal route, Ceram. Int. 40 (2014) 6203-6209.
[61] P. Nguyen Dang, L.H. Hoang, X.-B. Chen, M.-H. Kong, H.-C. Wen, W.C. Chou, Study of photocatalytic activities of Bi_2WO_6 nanoparticles synthesized by fast microwave-assisted method, J. Alloys Compd. 647 (2015) 123-128.
[62] M. Shang, W.Z. Wang, H.L. Xu, New Bi_2WO_6 Nanocages with High Visible-Light-Driven Photocatalytic Activities Prepared in Refluxing EG, Cryst. Growth Des. 9 (2009) 991-996.
[63] Y.Y. Wang, W.J. Jiang, W.J. Luo, X.J. Chen, Y.F. Zhu, Ultrathin nanosheets g-C_3N_4@Bi_2WO_6 core-shell structure via low temperature reassembled strategy to promote photocatalytic activity, Appl. Catal. B: Environ. 237 (2018) 633-640.
[64] L. Yuan, K.Q. Lu, F. Zhang, X.Z. Fu, Y.J. Xu, Unveiling the interplay between light-driven CO_2 photocatalytic reduction and carbonaceous residues decomposition: A case study of Bi_2WO_6-TiO_2 binanosheets, Appl. Catal. B: Environ. 237 (2018) 424-431.
[65] Q. Wang, Z.Q. Liu, D.M. Liu, G.S. Liu, M. Yang, F.Y. Cui, W. Wang, Ultrathin two-dimensional $BiOBr_xI_{1-x}$ solid solution with rich oxygen vacancies for enhanced visible-light-driven photoactivity in environmental remediation, Appl. Catal. B: Environ. 236 (2018) 222-232.
[66] Y. Wu, H. Wang, W.G. Tu, Y. Liu, S.Y. Wu, Y.Z. Tan, J.W. Chew, Construction of hierarchical 2D-2D $Zn_3In_2S_6$/fluorinated polymeric carbon nitride nanosheets

photocatalyst for boosting photocatalytic degradation and hydrogen production performance, Appl. Catal. B: Environ. 233 (2018) 58-69.
[67] Y.J. Yuan, Z.J. Li, S.T. Wu, D.Q. Chen, L.X. Yang, D.P. Cao, W.G. Tu, Z.T. Yu, Z.G. Zou, Role of two-dimensional nanointerfaces in enhancing the photocatalytic performance of 2D-2D MoS_2/CdS photocatalysts for H_2 production, Chem. Eng. J. 350 (2018) 335-343.
[68] F. Lei, Y. Sun, K. Liu, S. Gao, L. Liang, B. Pan, Y. Xie, Oxygen vacancies confined in ultrathin indium oxide porous sheets for promoted visible-light water splitting, J. Am. Chem. Soc. 136 (2014) 6826-6829.
[69] H. Huang, R. Cao, S. Yu, K. Xu, W. Hao, Y. Wang, F. Dong, T. Zhang, Y. Zhang, Single-unit-cell layer established Bi_2WO_6 3D hierarchical architectures: Efficient adsorption, photocatalysis and dye-sensitized photoelectrochemical performance, Appl. Catal. B: Environ. 219 (2017) 526-537.
[70] C. Zhang, Y.F. Zhu, Synthesis of square Bi_2WO_6 nanoplates as high-activity visible-light-driven photocatalysts, Chem. Mater. 17 (2005) 3537-3545.
[71] X.J. Wang, L.L. Chang, J.R. Wang, N.N. Song, H.L. Liu, X.L. Wan, Facile hydrothermal synthesis of Bi_2WO_6 microdiscs with enhanced photocatalytic activity, Appl. Surf. Sci. 270 (2013) 685-689.
[72] Y. Liu, H. Lv, J. Hu, Z. Li, Synthesis and characterization of Bi_2WO_6 nanoplates using egg white as a biotemplate through sol-gel method, Mater. Lett. 139 (2015) 401-404.
[73] Y. Zhou, Y. Zhang, M. Lin, J. Long, Z. Zhang, H. Lin, J.C.S. Wu, X. Wang, Monolayered Bi_2WO_6 nanosheets mimicking heterojunction interface with open surfaces for photocatalysis, Nat. Commun. 6 (2015) 8340.
[74] K. Matras-Postolek, A. Zaba, E.M. Nowak, P. Dabczynski, J. Rysz, J. Sanetra, Formation and characterization of one-dimensional ZnS nanowires for ZnS/P3HT hybrid polymer solar cells with improved efficiency, Appl. Surf. Sci. 451 (2018) 180-190.
[75] X.N. Liu, Q.F. Lu, J.H. Liu, Electrospinning preparation of one-dimensional ZnO/Bi_2WO_6 heterostructured sub-microbelts with excellent photocatalytic performance, J. Alloys Compd. 662 (2016) 598-606.
[76] X. Lin, Z. Liu, X. Guo, C. Liu, H. Zhai, Q. Wang, L. Chang, Controllable synthesis and photocatalytic activity of spherical, flower-like and nanofibrous bismuth tungstates, Mater. Sci. Eng: B 188 (2014) 35-42.
[77] S.-J. Liu, Y.-F. Hou, S.-L. Zheng, Y. Zhang, Y. Wang, One-dimensional hierarchical Bi_2WO_6 hollow tubes with porous walls: synthesis and photocatalytic property, CrystEngComm 15 (2013) 4124-4130.
[78] S. Xu, D. Fu, K. Song, L. Wang, Z. Yang, W. Yang, H. Hou, One-dimensional WO_3/$BiVO_4$ heterojunction photoanodes for efficient photoelectrochemical water splitting, Chem. Eng. J. 349 (2018) 368-375.
[79] G. Dong, Y. Zhang, Y. Bi, The synergistic effect of Bi_2WO_6 nanoplates and Co_3O_4 cocatalysts for enhanced photoelectrochemical properties, J. Mater. Chem. A 5 (2017) 20594-20597.
[80] G. Zhang, Z. Hu, M. Sun, Y. Liu, L. Liu, H. Liu, C. Huang, J. Qu, J. Li,

Formation of Bi_2WO_6 Bipyramids with Vacancy Pairs for Enhanced Solar-Driven Photoactivity, Adv. Funct. Mater. 25 (2015) 3726-3734.
[81] T. Hu, H. Li, N. Du, W. Hou, Iron-Doped Bismuth Tungstate with an Excellent Photocatalytic Performance, ChemCatChem 10 (2018) 3040-3048.
[82] J. de Boor, T. Dasgupta, U. Saparamadu, E. Muller, Z.F. Ren, Recent progress in p-type thermoelectric magnesium silicide based solid solutions, Mater. Today Energy (Netherlands) 4 (2017) 105-121.
[83] H.Y. Zhang, C.Y. Xin, X.T. Wang, K. Wang, Facile synthesis of $Cd_{0.2}Zn_{0.8}S$-ethylenediamine hybrid solid solution and its improved photocatalytic performance, Int. J. Hydrogen Energy 41 (2016) 12019-12028.
[84] A.V. Lebedev, S.A. Avanesov, T.M. Yunalan, V.A. Klimenko, B.V. Ignatyev, V.A. Isaev, Phase equilibria diagrams, crystal growth peculiarities and Raman investigations of lead and sodium-bismuth tungstate-molybdate solid solutions, Opt. Mater. 52 (2016) 203-211.
[85] W.Q. Li, X.G. Ding, H.T. Wu, H. Yang, $Bi_2Mo_xW_{1-x}O_6$ solid solutions with tunable band structure and enhanced visible-light photocatalytic activities, Appl. Surf. Sci. 447 (2018) 636-647.
[86] B.D. Liu, J. Li, W.J. Yang, X.L. Zhang, X. Jiang, Y. Bando, Semiconductor Solid-Solution Nanostructures: Synthesis, Property Tailoring, and Applications, Small 13 (2017) 1701998.
[87] D.D. Tune, B.S. Flavel, Advances in Carbon Nanotube–Silicon Heterojunction Solar Cells, Adv. Energy Mater. 8 (2018) 1703241.
[88] P.F. Xu, X.F. Shen, L. Luo, Z. Shi, Z.X. Liu, Z.G. Chen, M.F. Zhu, L.S. Zhang, Preparation of TiO_2/Bi_2WO_6 nanostructured heterojunctions on carbon fibers as a weaveable visible-light photocatalyst/photoelectrode, Environ. Sci. Nano 5 (2018) 327-337.
[89] K. Zhang, J. Wang, W. Jiang, W. Yao, H. Yang, Y. Zhu, Self-assembled perylene diimide based supramolecular heterojunction with Bi_2WO_6 for efficient visible-light-driven photocatalysis, Appl. Catal. B: Environ. 232 (2018) 175-181.
[90] Y.N. Wang, Y.Q. Zeng, X.Y. Chen, Q.Y. Wang, L.N. Guo, S.L. Zhang, Q. Zhong, One-step hydrothermal synthesis of a novel 3D $BiFeWO_x$/Bi_2WO_6 composite with superior visible-light photocatalytic activity, Green Chem. 20 (2018) 3014-3023.
[91] D.L. Jiang, W.X. Ma, P. Xiao, L.Q. Shao, D. Li, M. Chen, Enhanced photocatalytic activity of graphitic carbon nitride/carbon nanotube/Bi_2WO_6 ternary Z-scheme heterojunction with carbon nanotube as efficient electron mediator, J. Colloid Interface Sci. 512 (2018) 693-700.
[92] D. Huang, X. Yan, M. Yan, G. Zeng, C. Zhou, J. Wan, M. Cheng, W. Xue, Graphitic Carbon Nitride-Based Heterojunction Photoactive Nanocomposites: Applications and Mechanism Insight, ACS Appl. Mater. Inter. 10 (2018) 21035-21055.
[93] B. Li, C. Lai, G. Zeng, L. Qin, H. Yi, D. Huang, C. Zhou, X. Liu, M. Cheng, P. Xu, C. Zhang, F. Huang, S. Liu, Facile Hydrothermal Synthesis of Z-scheme $Bi_2Fe_4O_9$/Bi_2WO_6 Heterojunction Photocatalyst with Enhanced Visible-Light Photocatalytic Activity, ACS Appl. Mater. Inter. 10 (2018) 18824-18836.

[94] C. Zhang, J. Ren, J. Hua, L. Xia, J. He, D. Huo, Y. Hu, Multifunctional Bi_2WO_6 nanoparticles for CT-guided photothermal and oxygen-free photodynamic therapy, ACS Appl. Mater. Inter. 10 (2018) 1132-1146.
[95] F. Xu, H.M. Chen, C.Y. Xu, D.P. Wu, Z.Y. Gao, Q. Zhang, K. Jiang, Ultra-thin Bi_2WO_6 porous nanosheets with high lattice coherence for enhanced performance for photocatalytic reduction of Cr(VI), J. Colloid Interface Sci. 525 (2018) 97-106.
[96] Y.Y. Zhao, Y.B. Wang, E.Z. Liu, J. Fan, X.Y. Hu, Bi_2WO_6 nanoflowers: An efficient visible light photocatalytic activity for ceftriaxone sodium degradation, Appl. Surf. Sci. 436 (2018) 854-864.
[97] J. Liu, Q. Han, L. Chen, J. Zhao, C. Streb, Y. Song, Aggregation of Giant Cerium-Bismuth Tungstate Clusters into a 3D Porous Framework with High Proton Conductivity, Angew. Chem. Int. Ed. 57 (2018) 8416-8420.
[98] Y.Z. Wu, J. Ward-Bond, D.L. Li, S.H. Zhang, J.F. Shi, Z.Y. Jiang, g-C_3N_4@alpha-Fe_2O_3/C Photocatalysts: Synergistically Intensified Charge Generation and Charge Transfer for NADH Regeneration, ACS Catal. 8 (2018) 5664-5674.
[99] X. Zhao, H. Liu, Y. Shen, J. Qu, Photocatalytic reduction of bromate at C_{60} modified Bi_2MoO_6 under visible light irradiation, Appl. Catal. B: Environ. 106 (2011) 63-68.
[100] L. Yu, S. Ruan, X. Xu, R. Zou, J. Hu, One-dimensional nanomaterial-assembled macroscopic membranes for water treatment, Nano Today 17 (2017) 79-95.
[101] J. Di, J. Xia, Y. Ge, H. Li, H. Ji, H. Xu, Q. Zhang, H. Li, M. Li, Novel visible-light-driven CQDs/Bi_2WO_6 hybrid materials with enhanced photocatalytic activity toward organic pollutants degradation and mechanism insight, Appl. Catal. B: Environ. 168 (2015) 51-61.
[102] R. Wang, K.-Q. Lu, F. Zhang, Z.-R. Tang, Y.-J. Xu, 3D carbon quantum dots/graphene aerogel as a metal-free catalyst for enhanced photosensitization efficiency, Appl. Catal. B: Environ. 233 (2018) 11-18.
[103] Y.T. Li, L.A. Zhang, Y. Qin, F.Q. Chu, Y. Kong, Y.X. Tao, Y.X. Li, Y.F. Bu, D. Ding, M.L. Liu, Crystallinity Dependence of Ruthenium Nanocatalyst toward Hydrogen Evolution Reaction, ACS Catal. 8 (2018) 5714-5720.
[104] R. Rajendran, K. Varadharajan, V. Jayaraman, B. Singaram, J. Jeyaram, Photocatalytic degradation of metronidazole and methylene blue by PVA-assisted Bi_2WO_6-CdS nanocomposite film under visible light irradiation, Applied Nanoscience 8 (2018) 61-78.
[105] J.L. Zhang, Z. Ma, Enhanced visible-light photocatalytic performance of Ag_3VO_4/Bi_2WO_6 heterojunctions in removing aqueous dyes and tetracycline hydrochloride, J. Taiwan Inst. Chem. Eng. 78 (2017) 212-218.
[106] L.Y. Liang, Y. Tursun, A. Nulahong, T. Dilinuer, A. Tunishaguli, G. Gao, A. Abulikemu, K. Okitsu, Preparation and sonophotocatalytic performance of hierarchical Bi_2WO_6 structures and effects of various factors on the rate of Rhodamine B degradation, Ultrason. Sonochem. 39 (2017) 93-100.
[107] F.-Y. Liu, Y.-R. Jiang, C.-C. Chen, W.W. Lee, Novel synthesis of $PbBiO_2Cl$/BiOCl nanocomposite with enhanced visible-driven-light photocatalytic activity, Catal. Today 300 (2018) 112-123.

[108] S. Dong, X. Ding, T. Guo, X. Yue, X. Han, J. Sun, Self-assembled hollow sphere shaped Bi_2WO_6/RGO composites for efficient sunlight-driven photocatalytic degradation of organic pollutants, Chem. Eng. J. 316 (2017) 778-789.
[109] F. Zhang, Y.C. Zhang, G.S. Zhang, Z.J. Yang, D.D. Dionysiou, A.P. Zhu, Exceptional synergistic enhancement of the photocatalytic activity of SnS_2 by coupling with polyaniline and N-doped reduced graphene oxide, Appl. Catal. B: Environ. 236 (2018) 53-63.
[110] H. Yi, D. Huang, L. Qin, G. Zeng, C. Lai, M. Cheng, S. Ye, B. Song, X. Ren, X. Guo, Selective prepared carbon nanomaterials for advanced photocatalytic application in environmental pollutant treatment and hydrogen production, Appl. Catal. B: Environ. 239 (2018) 408-424.
[111] X. Li, S.S. Liu, D. Cao, R. Mao, X. Zhao, Synergetic activation of H_2O_2 by photo-generated electrons and cathodic Fenton reaction for enhanced self-driven photoelectrocatalytic degradation of organic pollutants, Appl. Catal. B: Environ. 235 (2018) 1-8.
[112] W.J. Ren, J.K. Gao, C. Lei, Y.B. Xie, Y.R. Cai, Q.Q. Ni, J.M. Yao, Recyclable metal-organic framework/cellulose aerogels for activating peroxymonosulfate to degrade organic pollutants, Chem. Eng. J. 349 (2018) 766-774.
[113] E.T. Martin, C.M. McGuire, M.S. Mubarak, D.G. Peters, Electroreductive Remediation of Halogenated Environmental Pollutants, Chem. Rev. 116 (2016) 15198-15234.
[114] J. Wang, L. Tang, G. Zeng, Y. Deng, H. Dong, Y. Liu, L. Wang, B. Peng, C. Zhang, F. Chen, 0D/2D interface engineering of carbon quantum dots modified Bi_2WO_6 ultrathin nanosheets with enhanced photoactivity for full spectrum light utilization and mechanism insight, Appl. Catal. B: Environ. 222 (2018) 115-123.
[115] L. Xu, J. Sun, Recent Advances in the Synthesis and Application of Two-Dimensional Zeolites, Adv. Energy Mater. 6 (2016) 1600441.
[116] R.S. Wang, B.X. Li, Y. Xiao, X.Q. Tao, X.T. Su, X.P. Dong, Optimizing Pd and Au-Pd decorated Bi_2WO_6 ultrathin nanosheets for photocatalytic selective oxidation of aromatic alcohols, J. Catal. 364 (2018) 154-165.
[117] M. Cantarella, A. Di Mauro, A. Gulino, L. Spitaleri, G. Nicotra, V. Privitera, G. Impellizzeri, Selective photodegradation of paracetamol by molecularly imprinted ZnO nanonuts, Appl. Catal. B: Environ. 238 (2018) 509-517.
[118] A.J. Han, H.W. Zhang, G.K. Chuah, S. Jaenicke, Influence of the halide and exposed facets on the visible-light photoactivity of bismuth oxyhalides for selective aerobic oxidation of primary amines, Appl. Catal. B: Environ. 219 (2017) 269-275.
[119] R. Ciriminna, R. Delisi, F. Parrino, L. Palmisano, M. Pagliaro, Tuning the photocatalytic activity of bismuth wolframate: towards selective oxidations for the biorefinery driven by solar-light, Chem. Commun. 53 (2017) 7521-7524.
[120] J. Yang, X.H. Wang, Y.M. Chen, J. Dai, S.H. Sun, Enhanced photocatalytic activities of visible-light driven green synthesis in water and environmental remediation on Au/Bi_2WO_6 hybrid nanostructures, RSC Adv. 5 (2015) 9771-9782.
[121] Y. Zhang, Y.-J. Xu, Bi_2WO_6: A highly chemoselective visible light photocatalyst toward aerobic oxidation of benzylic alcohols in water, RSC Adv. 4 (2014) 2904-

2910.
[122] P. Chen, L. Chen, Y. Zeng, F. Ding, X. Jiang, N. Liu, C.T. Au, S.F. Yin, Three-dimension hierarchical heterostructure of $CdWO_4$ microrods decorated with Bi_2WO_6 nanoplates for high-selectivity photocatalytic benzene hydroxylation to phenol, Appl. Catal. B: Environ. 234 (2018) 311-317.
[123] A. Dasgupta, L.P. Rajukumar, C. Rotella, Y. Lei, M. Terrones, Covalent three-dimensional networks of graphene and carbon nanotubes: synthesis and environmental applications, Nano Today 12 (2017) 116-135.
[124] J. Li, X. Wang, G. Zhao, C. Chen, Z. Chai, A. Alsaedi, T. Hayat, X. Wang, Metal-organic framework-based materials: superior adsorbents for the capture of toxic and radioactive metal ions, Chem. Soc. Rev. 47 (2018) 2322-2356.
[125] Y. Zhou, X.J. Zhang, Q. Zhang, F. Dong, F. Wang, Z. Xiong, Role of graphene on the band structure and interfacial interaction of Bi_2WO_6/graphene composites with enhanced photocatalytic oxidation of NO, J. Mater. Chem. A 2 (2014) 16623-16631.
[126] J. Wan, X. Du, R. Wang, E. Liu, J. Jia, X. Bai, X. Hu, J. Fan, Mesoporous nanoplate multi-directional assembled Bi_2WO_6 for high efficient photocatalytic oxidation of NO, Chemosphere 193 (2018) 737-744.
[127] Y.-J. Yuan, D.-Q. Chen, X.-F. Shi, J.-R. Tu, B. Hu, L.-X. Yang, Z.-T. Yu, Z.-G. Zou, Facile fabrication of “green” SnS_2 quantum dots/reduced graphene oxide composites with enhanced photocatalytic performance, Chem. Eng. J. 313 (2017) 1438-1446.
[128] Y. Li, Z. Liu, Y. Wu, J. Chen, J. Zhao, F. Jin, P. Na, Carbon dots-TiO_2 nanosheets composites for photoreduction of Cr(VI) under sunlight illumination: Favorable role of carbon dots, Appl. Catal. B: Environ. 224 (2018) 508-517.
[129] Y.Z. Zhang, S.C. Lin, J.Q. Qiao, D. Kolodynska, Y.M. Ju, M.W. Zhang, M.F. Cai, D.Y. Deng, D.D. Dionysiou, Malic acid-enhanced chitosan hydrogel beads (mCHBs) for the removal of Cr(VI) and Cu(II) from aqueous solution, Chem. Eng. J. 353 (2018) 225-236.
[130] Z. Lv, H. Zhou, H. Liu, B. Liu, M. Liang, H. Guo, Controlled assemble of oxygen vacant CeO_2@Bi_2WO_6 hollow magnetic microcapsule heterostructures for visible-light photocatalytic activity, Chem. Eng. J. 330 (2017) 1297-1305.
[131] Z.Y. Jiang, X.H. Zhang, Z.M. Yuan, J.C. Chen, B.B. Huang, D.D. Dionysiou, G.H. Yang, Enhanced photocatalytic CO_2 reduction via the synergistic effect between Ag and activated carbon in TiO_2/AC-Ag ternary composite, Chem. Eng. J. 348 (2018) 592-598.
[132] S. Sato, T. Morikawa, T. Kajino, O. Ishitani, A highly efficient mononuclear iridium complex photocatalyst for CO_2 reduction under visible light, Angew. Chem. Int. Ed. Engl. 52 (2013) 988-992.
[133] J.L. Lin, Z.M. Pan, X.C. Wang, Photochemical Reduction of CO_2 by Graphitic Carbon Nitride Polymers, ACS Sustain. Chem. Eng. 2 (2014) 353-358.
[134] H. Takeda, H. Koizumi, K. Okamoto, O. Ishitani, Photocatalytic CO_2 reduction using a Mn complex as a catalyst, Chem. Commun. 50 (2014) 1491-1493.
[135] H. Cheng, B. Huang, Y. Liu, Z. Wang, X. Qin, X. Zhang, Y. Dai, An anion exchange approach to Bi_2WO_6 hollow microspheres with efficient visible light

photocatalytic reduction of CO_2 to methanol, Chem. Commun. 48 (2012) 9729-9731.
[136] Y. Zhou, Z.P. Tian, Z.Y. Zhao, Q. Liu, J.H. Kou, X.Y. Chen, J. Gao, S.C. Yan, Z.G. Zou, High-Yield Synthesis of Ultrathin and Uniform Bi_2WO_6 Square Nanoplates Benefitting from Photocatalytic Reduction of CO_2 into Renewable Hydrocarbon Fuel under Visible Light, ACS Appl. Mater. Inter. 3 (2011) 3594-3601.
[137] M.L. Li, L.X. Zhang, X.Q. Fan, Y.J. Zhou, M.Y. Wu, J.L. Shi, Highly selective CO_2 photoreduction to CO over g-C_3N_4/Bi_2WO_6 composites under visible light, J. Mater. Chem. A 3 (2015) 5189-5196.
[138] X.J. Zheng, C.L. Li, M. Zhao, Z. Zheng, L.F. Wei, F.H. Chen, X.L. Li, Photocatalytic degradation of butyric acid over Cu_2O/Bi_2WO_6 composites for simultaneous production of alkanes and hydrogen gas under UV irradiation, Int. J. Hydrogen Energy 42 (2017) 7917-7929.
[139] L.N. Qiao, H.C. Wang, Y.D. Luo, H.M. Xu, J.P. Ding, S. Lan, Y. Shen, Y.H. Lin, C.W. Nan, Generation of hydrogen under visible light irradiation with enhanced photocatalytic activity of Bi_2WO_6/$Cu_{1.8}Se$ for organic pollutants under Vis-NIR light reign, J. Am. Ceram. Soc. 101 (2018) 3015-3025.
[140] J.K. Kim, G.D. Park, J.H. Kim, S.K. Park, Y.C. Kang, Rational Design and Synthesis of Extremely Efficient Macroporous $CoSe_2$-CNT Composite Microspheres for Hydrogen Evolution Reaction, Small 13 (2017) 1700068.
[141] S. Zhang, L. Wang, C. Liu, J. Luo, J. Crittenden, X. Liu, T. Cai, J. Yuan, Y. Pei, Y. Liu, Photocatalytic wastewater purification with simultaneous hydrogen production using MoS_2 QD-decorated hierarchical assembly of $ZnIn_2S_4$ on reduced graphene oxide photocatalyst, Water Res. 121 (2017) 11-19.
[142] A. Rauf, M. Ma, S. Kim, M. Shah, C.H. Chung, J.H. Park, P.J. Yoo, Mediator- and co-catalyst-free direct Z-scheme composites of Bi_2WO_6-Cu_3P for solar-water splitting, Nanoscale 10 (2018) 3026-3036.
[143] Z.Y. Fan, H.J. Shi, H.Y. Zhao, J.Z. Cai, G.H. Zhao, Application of carbon aerogel electrosorption for enhanced Bi_2WO_6 photoelectrocatalysis and elimination of trace nonylphenol, Carbon 126 (2018) 279-288.
[144] S.B. Chen, H. Nan, X. Zhang, Y.T. Yan, Z. Zhou, Y. Zhang, K. Wang, One-step hydrothermal treatment to fabricate Bi_2WO_6-reduced graphene oxide nanocomposites for enhanced visible light photoelectrochemical performance, Journal of Materials Chemistry B 5 (2017) 3718-3727.
[145] J. Wang, L. Tang, G. Zeng, Y. Deng, Y. Liu, L. Wang, Y. Zhou, Z. Guo, J. Wang, C. Zhang, Atomic scale g-C_3N_4/Bi_2WO_6 2D/2D heterojunction with enhanced photocatalytic degradation of ibuprofen under visible light irradiation, Appl. Catal. B: Environ. 209 (2017) 285-294.
[146] H.W. Huang, R.R. Cao, S.X. Yu, K. Xu, W.C. Hao, Y.G. Wang, F. Dong, T.R. Zhang, Y.H. Zhang, Single-unit-cell layer established Bi_2WO_6 3D hierarchical architectures: Efficient adsorption, photocatalysis and dye-sensitized photoelectrochemical performance, Appl. Catal. B: Environ. 219 (2017) 526-537.
[147] G.J. Dong, Y.J. Zhang, Y.P. Bi, The synergistic effect of Bi_2WO_6 nanoplates and Co_3O_4 cocatalysts for enhanced photoelectrochemical properties, J. Mater. Chem. A 5 (2017) 20594-20597.

[148] K. Kadeer, Y. Tursun, T. Dilinuer, K. Okitsu, A. Abulizi, Sonochemical preparation and photocatalytic properties of CdS QDs/Bi_2WO_6 3D heterojunction, Ceram. Int. 44 (2018) 13797-13805.

Table 1 Summary of pure nano-structured BWO and their photocatalytic application.

Dimension	Fabrication	Structure and morphology	BET /m^2g^{-1}	Morphology-dependent property	Target /BWO dosage Photocatalytic efficiency	Ref
3D	Hydrothermal process	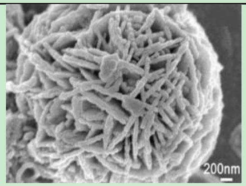	10.7	Layered flower-like spherical fromed by nanoplates.	20 mg L^{-1} 2,4,6-trichlorophenol /1 g L^{-1} 52% in 120 min	[53]
	hydrothermal process	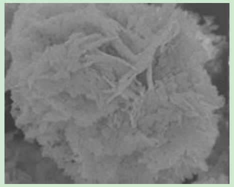	35.3	Layered flower-like spherical with larger surface area.	20 mg L^{-1} RhB /0.1 g L^{-1} 60% in 60 min	[58]
	Sol-gel hydrothermal process	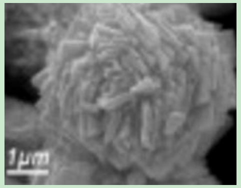	14.2	Hierarchical microspheres with high crystallization.	10 mg L^{-1} MB /0.67 g L^{-1} ~80% in 100 min	[60]
	Microwave	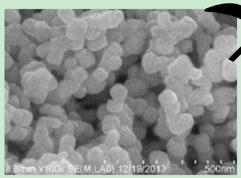	14.[illegible]	Nanoparticles (~60 nm) showed high transportation efficiency of photo-generated charges.	10^{-5} M MB /1 g L^{-1} ~92% in 180 min	[61]

	Hydrothermal process	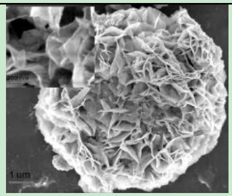	55.1	Single-unit-cell layer established 3D hierarchical BWO showed high adsorptivity.	0.01mM RhB /1 g L^{-1} 93.1 % in 60 min	[69]
2D	Sol-gel process	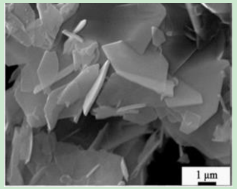	3.5	Nanoplate with enhanced multiple reflections of visible light.	5 mg L^{-1} RhB /1 g L^{-1} 91.1% in 120 min	[72]
	Bottom-up hydrothermal process	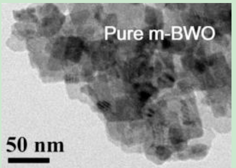	43.0	Monolayer nanosheets showed rapid separation of photoexcited e^- - h^+ pairs.	10 mg L^{-1} MO /1 g L^{-1} 47.3% in 120 min	[114]
	Hydrothermal process	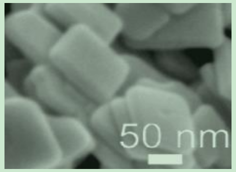	5.6	Ultrathin square nanoplate showed rapid move of charge carriers.	Reduction of CO_2 to CH_4 1.1 μmol g^{-1} h^{-1} of CH_4	[136]
1D	Solvothermal process	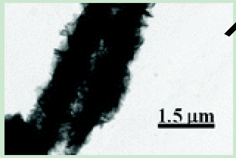	32.0	hollow structure improved the charge collection.	10^{-5} M RhB / 0.5 g L^{-1} 99.0% in 90 min	[77]

5 Table 2 Environmental application of modified nano-structured BWO photocatalysts.

Photocatalyst	Target	Dosage of photocatalyst	Photocatalytic Efficiency	The proposed reason for improved performances	Ref
Hemin-BWO	10 mg L^{-1} RhB	0.1 g L^{-1}	99.5% in 60 min	Hemin act as an electron shuttle that transferred the photogenerated electrons of BWO.	[58]
$Bi_2Fe_4O_9$/BWO	10 mg L^{-1} RhB	0.3 g L^{-1}	99.9% in 90 min	The formation of Z-scheme heterojunction enhances the separation of photogenerated charge carriers.	[93]
Ag_3VO_4/BWO	10 mg L^{-1} MO[a] 10 mg L^{-1} RhB 10 mg L^{-1} MB[a]	0.6 g L^{-1}	84.5% in 60 min 99.8% in 15 min 99.8% in 15 min	The formation of Ag_3VO_4/BWO heterojunction facilitates the separation and migration of photogenerated carriers.	[105]
RGO/BWO	10 mg L^{-1} MO	0.5 g L^{-1}	80.1% in 480 min	RGO has a positive impact on the electronic properties of BWO.	[108]
CBW	10 mg L^{-1} MO	1.0 g L^{-1}	80.[illegible]% in 120 min	CQDs act as an electron reservoir for trapping photoexcited electrons to separate the electron-hole pairs.	[114]
$g-C_3N_4$/BWO	25 μM IBF[a]	0.2 g L^{-1}	96.1% in 60 min	The formation of ultrathin heterojunctions enhances the charge transfer across substantial heterojunction interface.	[145]

BWO/PDI	5 ppm phenol	0.5 g L^{-1}	68.2% in 180 min	Self-assembled PDI and BWO surface hybridization to promote the separation of photogenerated carriers, electrons in the LUMO orbit of PDI are injected into the conduction band of the BWO, produced a superoxide radical-based visible light degradation activity.	[89]
Ag_3VO_4/BWO	20 mg L^{-1} TC^a	0.6 g L^{-1}	71.5% in 15 min	The formation of Ag_3VO_4/BWO heterojunction facilitates the separation and migration of photogenerated carriers.	[105]
CBW	10 mg L^{-1} BPA	1.0 g L^{-1}	99.9% in 60 min	CQDs act as an electron reservoir for trapping photoexcited electrons to separate the electron-hole pairs.	[114]
Au(x)Pd(x)-BWO	Selective oxidation of 0.05 mmol benzylic alcohols to aldehydes	5.0 mg	1.5 mmol h^{-1} g^{-1}	The multi-component interactions between metals and between metals and semiconductor improved the photoabsorption and charge carriers separation.	[116]
Flower-like BWO	Selective oxidation of 0.1 mmol benzylic alcohols to aldehydes	3.0 mg	0.6 mmol h^{-1} g^{-1}	The integrative factors associated with morphology have an effect on the selective oxidation, including the slight oxidation ability and stronger adsorption on benzylic alcohols than aldehydes.	[121]

BCW	Selective oxidation of 0.5 mmol benzene to phenol	50.0 mg	0.2 mmol h^{-1} g^{-1}	The unique hierarchical heterostructure improves the photoabsorption and charge carriers separation.	[122]
BWO-180-C	2 ppm NO 400 mL/min	0.1 g	95.2% in 2 min	Appropriate pores size and the special interconnected porous networks of hierarchical multi-directional mesoporous structures improve the photocatalytic efficiency, durability, and reusability.	[126]
CeO_2@BWO	8 mgL^{-1} Cr(VI) 4.78 mM cyanide	0.5 g L^{-1}	99.6% in 60 min 98.3% in 60 min	The oxygen vacancy, heterostructures improved charge separation and interfacial charge transfer efficiency, and the hollow capsule of the photocatalyst improve the light efficiency significantly.	[130]
Single unit cell BWO	CH_4 production (0.5 mL min^{-1} CO_2)	0.2 g	75.0 μmol g^{-1} h^{-1}	Atomic layers afford abundant catalytic sites, increased two-dimensional conductivity, and superior structural stability.	[38]
BWO HMSs[a]	CH_4 production (0.2 mL min^{-1} CO_2)	0.2 g	16.3 μmol g^{-1} h^{-1}	Hollow microspheres possess large surface area and high CO_2 adsorption capacity.	[135]
$g\text{-}C_3N_4$/BWO	CO production	0.1 g	5.19 μmol g^{-1} h^{-1}	Z-scheme reaction of $g\text{-}C_3N_4$/BWO significantly promoted separation of photo-generated carriers under visible light irradiation.	[137]

Cu_2O/BWO	H_2 production	0.1 g was added in 450 mL distilled water	30.7μmol g^{-1} h^{-1}	Heterostructure of Cu_2O/BWO enhances light absorption and effective inhibition of recombination of photogenerated carriers.	[138]
BWO/$Cu_{1.8}$Se	H_2 production	0.1 g was added into 100 mL CR[a] solution (100 mg L^{-1})	30.1μmol g^{-1} h^{-1}	Bi_2WO_6/$Cu_{1.8}$Se heterojunction reveals good light absorption, suitable band gap structure, and effective separation of photogenerated electron–hole pairs.	[139]
BWO-Cu_3P	H_2 production	0.1 g was added in 80 ml of 0.5 M Na_2HPO_4/NaH_2PO_4 buffer solution	4.8μmol g^{-1} h^{-1}	Effective solid–solid contact plays an important role in the improved efficiency.	[142]

[a] MB, methylene blue; MO, methyl orange; IBF, ibuprofen; TC, tetracycline hydrochloride; BWO HMSs, BWO hollow microspheres; CR, congo red.